Appl. Math. Mech. -Engl. Ed., **46**(5), 965–988 (2025)

APPLIED MATHEMATICS AND MECHANICS (ENGLISH EDITION)

https://doi.org/10.1007/s10483-025-3248-7

Structural vibration control using nonlinear damping amplifier friction vibration absorbers*

S. CHOWDHURY†, S. ADHIKARI

Glasgow Computational Engineering Center, James Watt School of Engineering,
The University of Glasgow, Glasgow G12 8QQ, United Kingdom

(Received Dec. 13, 2024 / Revised Mar. 10, 2025)

Abstract This paper introduces damping amplifier friction vibration absorbers (DAFVAs), compound damping amplifier friction vibration absorbers (CDAFVAs), nested damping amplifier friction vibration absorbers (NDAFVAs), and levered damping amplifier friction vibration absorbers (LDAFVAs) for controlling the structural vibrations and addressing the limitations of conventional tuned mass dampers (TMDs) and friction-tuned mass dampers (FTMDs). The closed-form analytical solution for the optimized design parameters is obtained using the H_2 and H_∞ optimization approaches. The efficiency of the recently established closed-form equations for the optimal design parameters is confirmed by the analytical examination. The closed form formulas for the dynamic responses of the main structure and the vibration absorbers are derived using the transfer matrix formulations. The foundation is provided by the harmonic and random-white noise excitations. Moreover, the effectiveness of the innovative dampers has been validated through numerical analysis. The optimal DAFVAs, CDAFVAs, NDAFVAs, and LDAFVAs exhibit at least 30% lower vibration reduction capacity compared with the optimal TMD. To demonstrate the effectiveness of the damping amplification mechanism, the novel absorbers are compared with a conventional FTMD. The results show that the optimized novel absorbers achieve at least 91% greater vibration reduction than the FTMD. These results show how the suggested designs might strengthen the structure's resilience to dynamic loads.

Key words damping amplifier friction vibration absorber (DAFVA), compound damping amplifier friction vibration absorber (CDAFVA), nested damping amplifier friction vibration absorber (NDAFVA), levered damping amplifier friction vibration absorber (LDAFVA), H_2 and H_∞ optimization approaches

Chinese Library Classification O322
2010 Mathematics Subject Classification 34C15, 74H45

1 Introduction

Mechanical vibrations are dampened in amplitude by a tuned mass damper (TMD). It can be used in many different fields, such as electrical engineering, mechanical engineering, and civil

* Citation: CHOWDHURY, S. and ADHIKARI, S. Structural vibration control using nonlinear damping amplifier friction vibration absorbers. *Applied Mathematics and Mechanics* (*English Edition*), **46**(5), 965–988 (2025) https://doi.org/10.1007/s10483-025-3248-7

† Corresponding author, E-mail: Sudip.Chowdhury@glasgow.ac.uk

engineering[1]. The fundamental ideas, design issues, uses, and most recent developments in TMD technology will be examined in this literature review. The foundation of TMDs is the concept of damping and resonance. A mass, a spring, and a damper comprise a TMD. The device is tuned to the inherent frequency of the building that it is intended to safeguard[2]. The damper dissipates vibrational energy and lowers oscillation amplitudes when the TMD resonates out of phase with the vibrating structure. Finding the ideal mass ratio, tuning frequency, and damping coefficient is the initial step in designing a TMD. These elements are essential to guaranteeing the TMD's effectiveness in lowering vibrations[3]. The TMD needs to represent a moderate portion of the overall mass of the construction. Mass ratios typically fall between 1% and 10%. It is necessary to adjust the TMD to correspond with the primary structure's inherent frequency. The damper should dissipate enough energy without appreciably lessening the sensitivity of the TMD. TMDs are frequently used to lessen vibrations caused by wind, earthquakes, and human activity in a range of projects. According to many researchers, seismic elements are commonly observed in skyscrapers, bridges, and sports stadiums[4]. Tall buildings' sway caused by wind is lessened with the use of TMDs. Taipei 101 and Boston's John Hancock Tower are two notable examples. Equipment vibrations that can cause fatigue and failure are reduced by TMDs. They are frequently used in precision devices and engines[5].

TMDs significantly lessen structural vibrations but come with a number of disadvantages. The cost of designing, producing, and maintaining them is high. Design and integration are challenging due to TMDs' large footprint and structural weight[6]. Because of their narrow frequency range efficiency, they are not appropriate for variable dynamic loads. Accurate adjustment is necessary, and any changes to the characteristics of the structure may reduce its efficiency. The performance of TMDs can be impacted by temperature changes[7]. In addition, they might not be as predictable as vibrations caused by wind during complex earthquake events. In older structures, retrofitting TMDs can be difficult and disruptive. Moreover, the installation could obstruct a structure's ability to function normally or its aesthetic appeal[8]. TMDs are nevertheless a useful tool for reducing vibration in a range of applications, despite these drawbacks[9].

It will need a combination of technology improvement, legislative reform, and strategic planning to overcome the issues with TMDs. Here are a few ways to deal with these problems. Make research investments to create materials that will require fewer replacements over time and are less prone to environmental degradation[10]. Offer specialized isolation solutions for different kinds of buildings, such as ones with asymmetrical or taller construction. Provide readily adjustable, modular-TMD systems for retrofitting pre-existing structures. Provide basic isolation solutions that are space-efficient and nevertheless function, like compact or low-profile dampers[11]. High-tech seismic modeling and simulation tools can improve the accuracy of your forecasts and planning for extreme events. Integrate TMDs with other earthquake mitigation technologies, such as bracing systems or dampers, to maximize overall performance. Allow for movable utility and service connections to enable base-isolated constructions[12]. Early in the design process, confer with engineers and utility providers to make sure that all systems are compatible with TMDs. Incorporate architectural strategies, including dampening devices, to minimize swaying and restrict the visual movement of the building[13]. By providing analytical closed-form solutions for the ideal damper design parameters when constructing the structures, the bulk of the restrictions have been overcome. H_2 is one of the optimization strategies. This was used to analytically estimate the optimal design parameters for the dampers[14]. Stochastic analysis is necessary to account for random excitation in the H_2 optimization technique for TMDs, such as seismic ground motions, which are regarded as random processes. This calls for taking into account the statistical characteristics of the stimulus and the reactions[15]. This is a comprehensive description of how H_2 is used to maximize the TMD under random stimulation. Reducing the mean-square reactivity, or energy, of a base-isolated structure to random seismic excitations is a goal. Using random excitation, create frequency response functions

(FRFs) that illustrate the structure and TMD system. Use stochastic processes to solve the H_2 optimization issue[16]. Use performance evaluation techniques such as stochastic simulations and frequency-domain analysis to confirm resilience. The optimized system exhibits reduced peak and root-mean-square (RMS) responses in comparison with the non-optimized systems. In order to increase robustness against worst-case disturbances, the H_∞ optimization for TMDs seeks to minimize the peak value of the system's FRF[17]. The goal of this approach is to reduce the H_∞ norm, which represents the maximum system response at all frequencies, by constructing and solving an optimization problem. TMD characteristics such as the mass ratio, tuning frequency, and damping ratio are changed during the optimization process. Benefits include better structural stability due to decreased peak reactions and greater performance[18]. It can, however, be computationally taxing and sensitive to changes in parameters. Vibration control is enhanced in industries such as aerospace, automotive, and civil engineering by H_∞ optimization[19].

By using their inertial characteristics, inertial amplifiers, also referred to as mass amplification devices, increase forces or movements. This idea usually entails using mechanical leverage, resonance, or inertia to amp up small input forces or displacements into bigger, more useful outputs[20]. Here is a detailed description of the functions and uses of these devices. Tiny input forces are amplified by inertial amplifiers through the use of the inertia of a mass. Usually, this is achieved with mechanical systems that make use of the inertia of a bigger mass to produce a force or displacement that is proportionately greater[21]. Mechanical leverage, a system of levers or gears that transforms a small force exerted over a short distance into a bigger force supplied over a longer distance, is something that these machines are capable of employing. Another technique is resonance, in which a system is engineered to oscillate at a specific frequency. Modest periodic pressures applied at the resonant frequency have the potential to magnify the input by causing the system to accumulate bigger oscillations[22]. By measuring and controlling vibrations in machinery and structures, these tools lessen damage and enhance engineering performance. Inertial amplifiers are essential mass amplification devices in numerous scientific and technical applications. These devices amplify small inputs into bigger, more useful outputs through the utilization of resonance, mechanical leverage, and inertia. This makes it possible to measure and regulate forces and motion with greater accuracy[23]. In practice, the vibration attenuation capacity of the amplifier can be improved by damping the inertially amplified hosting structures. This leads to a change in the inertial amplifiers' frequency and an increase in effective damping, which could reduce the cost of producing vibration attenuation devices. The quantity of material needed has decreased as a result of the use of these amplifiers. Damping amplifiers, however, are not mentioned in the current research review. Moreover, there are currently no state-of-the-art damping amplifier friction vibration absorbers (DAFVAs) that can address every drawback of TMDs.

In this paper, the DAFVAs are designed to overcome their limitations and enhance their vibration reduction performance by inducing damping amplifiers inside the core material. Consequently, DAFVAs, compound damping amplifier friction vibration absorbers (CDAFVAs), nested damping amplifier friction vibration absorbers (NDAFVAs), and levered damping amplifier friction vibration absorbers (LDAFVAs) are shown. The closed-form analytic solution for the ideally designed parameters is produced using the H_2 and H_∞ optimization techniques. The effectiveness of the recently discovered closed-form equations for ideal design parameters is confirmed by the analytical study. The dynamic responses of the damper and main structure are found to have closed-form formulas through the use of the FRF. The basis excitations are the random-white noise and harmonic excitations. The novel dampers' ability to reduce vibration is contrasted with that of the conventional TMDs. The damping amplification mechanism of the novel absorbers is evaluated through a comparison with a conventional friction-tuned mass damper (FTMD) featuring a spring and dry friction damping[24].

2 DAFVAs

Conventional vibration absorbers are tested with additional damping amplifiers in order to overcome their existing drawbacks and enhance their performances. The structural diagrams of the single degree of freedom (SDOF) systems controlled by the DAFVAs, CDAFVAs, NDAFVAs, and LDAFVAs subjected to base excitation are shown in Figs. 1(a)–1(d). An application of Newton's second law is required in order to determine the equations of motion that govern the controlled system with an SDOF. It is possible to obtain the equations of motion for the system with an SDOF as follows:

$$m_{\mathrm{s}}\ddot{x}_{\mathrm{s}} = -k_{\mathrm{s}}(x_{\mathrm{s}} - u_{\mathrm{g}}) - c_{\mathrm{s}}(\dot{x}_{\mathrm{s}} - \dot{u}_{\mathrm{g}}) + k_{\mathrm{d}}(x_{\mathrm{d}} - x_{\mathrm{s}}) + \alpha m_{\mathrm{d}} g \mathrm{sgn}(\dot{x}_{\mathrm{d}} - \dot{x}_{\mathrm{s}}) + c_{\mathrm{d}}(\dot{x}_{\mathrm{d}} - \dot{x}_{\mathrm{s}}), \quad (1)$$

where x_{s} and x_{d} define the absolute displacements of the SDOF system and the novel dampers, respectively. u_{g} defines the base displacement. Now, consider $u_{\mathrm{d}} = x_{\mathrm{d}} - x_{\mathrm{s}}$ and $u_{\mathrm{s}} = x_{\mathrm{s}} - u_{\mathrm{g}}$, which are defined as the relative displacements of the dampers and the SDOF system, respectively. The relative displacements are substituted in Eq. (1),

$$m_{\mathrm{s}}\ddot{u}_{\mathrm{s}} + c_{\mathrm{s}}\dot{u}_{\mathrm{s}} + k_{\mathrm{s}}u_{\mathrm{s}} - \alpha m_{\mathrm{d}} g \mathrm{sgn}(\dot{u}_{\mathrm{d}}) - c_{\mathrm{d}}\dot{u}_{\mathrm{d}} - k_{\mathrm{d}}u_{\mathrm{d}} = -m_{\mathrm{s}}\ddot{u}_{\mathrm{g}}. \quad (2)$$

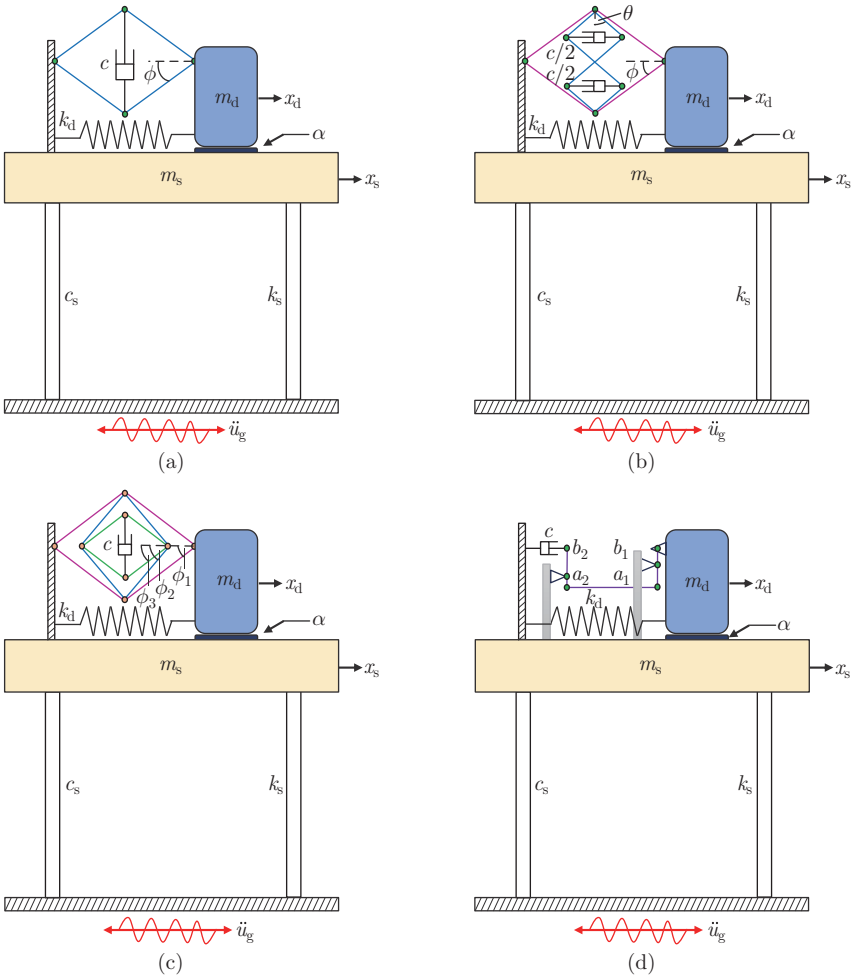

Fig. 1 The structural diagrams of the SDOF system controlled by the (a) DAFVA, (b) CDAFVA, (c) NDAFVA, and (d) LDAFVA subjected to base excitation (color online)

It is possible to obtain the equation of motion for the damper as

$$m_{\mathrm{d}}\ddot{x}_{\mathrm{d}} = -\alpha m_{\mathrm{d}} g \mathrm{sgn}(\dot{x}_{\mathrm{d}} - \dot{x}_{\mathrm{s}}) - c_{\mathrm{d}}(\dot{x}_{\mathrm{d}} - \dot{x}_{\mathrm{s}}) - k_{\mathrm{d}}(x_{\mathrm{d}} - x_{\mathrm{s}}). \tag{3}$$

Substituting the relative displacements into Eq. (3) yields

$$m_{\mathrm{d}}\ddot{u}_{\mathrm{d}} + m_{\mathrm{d}}\ddot{u}_{\mathrm{s}} + \alpha m_{\mathrm{d}} g \mathrm{sgn}(\dot{u}_{\mathrm{d}}) + c_{\mathrm{d}}\dot{u}_{\mathrm{d}} + k_{\mathrm{d}}u_{\mathrm{d}} = -m_{\mathrm{d}}\ddot{u}_{\mathrm{g}}, \tag{4}$$

where m_{d}, c_{d}, and k_{d} define the mass, damping, and stiffness of the DAFVAs, respectively. α defines the friction coefficient. u_{d} $(= x_{\mathrm{d}} - x_{\mathrm{s}})$ and u_{s} $(= x_{\mathrm{s}} - u_{\mathrm{g}})$ define the relative displacements of the damper and the SDOF system, respectively. The statistical linearization method applied to Eq. (1) is used to linearize each nonlinear element of the governing equation of motion in order to apply the H_2 optimization strategy. The H_2 optimization approach is used to provide an appropriate tuning of natural frequency to the controlled structures and to accurately determine the closed-form expressions of the optimal damper design parameters while accounting for the nonlinear hysteretic response of the controlled structure. The equivalent damping of the dampers is computed as

$$c_{\mathrm{eq}} = E\Big(\frac{\partial(\alpha m_{\mathrm{d}} g \mathrm{sgn}(\dot{u}_{\mathrm{d}}))}{\partial \dot{u}_{\mathrm{d}}}\Big) = \sqrt{\frac{2}{\pi}}\frac{\alpha m_{\mathrm{d}} g}{\sigma_{\dot{u}_{\mathrm{d}}}}. \tag{5}$$

Initially, c_{eq} has been considered zero to obtain the closed-form expression for $\sigma_{\dot{u}_{\mathrm{d}}}$. For each DAFVA, the value of c_{d} has been derived as follows.

DAFVAs:

$$c_{\mathrm{d}} = c\underbrace{\cot^2\phi}_{\vartheta} \tag{6}$$

with ϕ defining the inertial angle.

CDAFVAs:

$$c_{\mathrm{d}} = \underbrace{c\cot^2\phi\Big(\frac{\tan^2\theta}{4}\Big)}_{\vartheta} \tag{7}$$

with ϕ and θ defining the primary and secondary inertial angles, respectively.

NDAFVAs:

$$c_{\mathrm{d}} = c\underbrace{\cot^2\phi_1 \tan^2\phi_2 \cot^2\phi_3}_{\vartheta} \tag{8}$$

with ϕ_1, ϕ_2, and ϕ_3 defining the primary, secondary, and tertiary inertial angles, respectively.

LDAFVAs:

$$c_{\mathrm{d}} = c\underbrace{\Big(\frac{b_1}{a_1}\frac{b_2}{a_2}\Big)^2}_{\vartheta}, \tag{9}$$

where $\left(\frac{b_1}{a_1}\,\frac{b_2}{a_2}\right)$ defines the lever arm length ratio. ϑ defines the damping amplification factor. The value for c is derived as $c = 2m_{\mathrm{d}}\xi_{\mathrm{b}}\nu_{\mathrm{b}}$. The stiffness of the DADVAs is obtained as $k_{\mathrm{d}} = m_{\mathrm{d}}\nu_{\mathrm{b}}^2$. As the controlled SDOF system is subjected to base excitation, it may produce steady-state responses: $u_{\mathrm{s}} = U_{\mathrm{s}}\mathrm{e}^{\mathrm{i}\omega t}$, $u_{\mathrm{d}} = U_{\mathrm{d}}\mathrm{e}^{\mathrm{i}\omega t}$, and $\ddot{u}_{\mathrm{g}} = U_{\mathrm{g}}\mathrm{e}^{\mathrm{i}\omega t}$. We apply these steady-state responses to the second expressions of Eq. (2) and Eq. (4), and as a result, a transfer matrix is derived to

evaluate the displacement response of each unknown degree of freedom of the controlled SDOF system.

$$\begin{pmatrix} 2\xi_{\mathrm{s}}\nu_{\mathrm{s}}q+\nu_{\mathrm{s}}^2+q^2 & -2\mu_{\mathrm{d}}\xi_{\mathrm{b}}\nu_{\mathrm{b}}q\vartheta-\mu_{\mathrm{d}}\nu_{\mathrm{b}}^2 \\ \mu_{\mathrm{d}}q^2 & 2\mu_{\mathrm{d}}\xi_{\mathrm{b}}\nu_{\mathrm{b}}q\vartheta+\mu_{\mathrm{d}}\nu_{\mathrm{b}}^2+\mu_{\mathrm{d}}q^2 \end{pmatrix} \begin{pmatrix} U_{\mathrm{s}} \\ U_{\mathrm{d}} \end{pmatrix} = -\begin{pmatrix} 1 \\ \mu_{\mathrm{d}} \end{pmatrix} U_{\mathrm{g}}. \tag{10}$$

The displacement of the SDOF system is derived as

$$H_{\mathrm{s}} = \frac{U_{\mathrm{s}}}{U_{\mathrm{g}}}\bigg|_{q=\mathrm{i}\omega} = \frac{-2\mu_{\mathrm{d}}\xi_{\mathrm{b}}\nu_{\mathrm{b}}q\vartheta-2\nu_{\mathrm{b}}q\xi_{\mathrm{b}}\vartheta-\mu_{\mathrm{d}}\nu_{\mathrm{b}}^2-\nu_{\mathrm{b}}^2-q^2}{\Delta_{\mathrm{f}}}. \tag{11}$$

The displacement of the damper is derived as

$$H_{\mathrm{d}} = \frac{U_{\mathrm{d}}}{U_{\mathrm{g}}}\bigg|_{q=\mathrm{i}\omega} = \frac{-2\xi_{\mathrm{s}}\nu_{\mathrm{s}}q-\nu_{\mathrm{s}}^2}{\Delta_{\mathrm{f}}}. \tag{12}$$

The denominator of Eq. (11) and Eq. (12) is obtained as

$$\begin{aligned}\Delta_{\mathrm{f}} = {} & q^4+(2\nu_{\mathrm{b}}\xi_{\mathrm{b}}\vartheta\mu_{\mathrm{d}}+2\nu_{\mathrm{b}}\xi_{\mathrm{b}}\vartheta+2\xi_{\mathrm{s}}\nu_{\mathrm{s}})q^3+(4\nu_{\mathrm{b}}\nu_{\mathrm{s}}\xi_{\mathrm{b}}\xi_{\mathrm{s}}\vartheta+\mu_{\mathrm{d}}\nu_{\mathrm{b}}^2+\nu_{\mathrm{b}}^2+\nu_{\mathrm{s}}^2)q^2 \\ & +(2\nu_{\mathrm{b}}\nu_{\mathrm{s}}^2\xi_{\mathrm{b}}\vartheta+2\nu_{\mathrm{b}}^2\nu_{\mathrm{s}}\xi_{\mathrm{s}})q+\nu_{\mathrm{b}}^2\nu_{\mathrm{s}}^2,\end{aligned} \tag{13}$$

where $q=\mathrm{i}\omega$, and $\mathrm{i}\ (=\sqrt{-1})$ defines the imaginary number. ω defines the excitation frequency. $\mu_{\mathrm{d}}\ (=m_{\mathrm{d}}/m_{\mathrm{s}})$ defines the damper mass ratio. ξ_{s} and ξ_{b} define the damping ratios of the SDOF system and the absorber, respectively. ν_{b} and ν_{s} define the natural frequencies of the absorber and SDOF system, respectively.

2.1 H_2 optimization

The isolated SDOF system is subjected to random white excitation. H_2 optimization is applicable, and the standard deviation of the displacement of the SDOF system is derived using Eqs. (11) and (13).

2.1.1 Derivation of the optimal design parameters by considering $\xi_{\mathrm{s}} \neq 0$

The damping of the main structure is not considered zero for this study, i.e., $\xi_{\mathrm{s}} \neq 0$. Equation (13) is a fourth-order polynomial equation, and the entire controlled SDOF system is subjected to random white noise. Accordingly, H_2 optimization is applicable. The standard deviation of the displacement of the SDOF system is derived using Eqs. (11) and (13), which is expressed as

$$\begin{aligned}\sigma_{u_{\mathrm{s}}}^2 = {} & S_0\pi(4\nu_{\mathrm{s}}^2\xi_{\mathrm{b}}^3\nu_{\mathrm{b}}^2\vartheta^3\mu_{\mathrm{d}}^3+4\xi_{\mathrm{s}}\nu_{\mathrm{s}}\nu_{\mathrm{b}}^3\mu_{\mathrm{d}}^3\xi_{\mathrm{b}}^2\vartheta^2+12\nu_{\mathrm{s}}^2\xi_{\mathrm{b}}^3\nu_{\mathrm{b}}^2\vartheta^3\mu_{\mathrm{d}}^2+12\xi_{\mathrm{s}}\nu_{\mathrm{s}}\nu_{\mathrm{b}}^3\mu_{\mathrm{d}}^2\xi_{\mathrm{b}}^2\vartheta^2+4\xi_{\mathrm{s}}\nu_{\mathrm{s}}^3\nu_{\mathrm{b}}\mu_{\mathrm{d}}^2\xi_{\mathrm{b}}^2\vartheta^2 \\ & +12\nu_{\mathrm{s}}^2\xi_{\mathrm{b}}^3\nu_{\mathrm{b}}^2\vartheta^3\mu_{\mathrm{d}}+\mu_{\mathrm{d}}^4\nu_{\mathrm{b}}^4\xi_{\mathrm{b}}\vartheta+4\nu_{\mathrm{s}}^2\xi_{\mathrm{b}}\nu_{\mathrm{b}}^2\vartheta\xi_{\mathrm{s}}^2\mu_{\mathrm{d}}^2+12\xi_{\mathrm{s}}\nu_{\mathrm{s}}\nu_{\mathrm{b}}^3\xi_{\mathrm{b}}^2\vartheta^2\mu_{\mathrm{d}}+8\xi_{\mathrm{s}}\nu_{\mathrm{s}}^3\nu_{\mathrm{b}}\xi_{\mathrm{b}}^2\vartheta^2\mu_{\mathrm{d}} \\ & +4\nu_{\mathrm{s}}^2\xi_{\mathrm{b}}^3\nu_{\mathrm{b}}^2\vartheta^3+4\mu_{\mathrm{d}}^3\nu_{\mathrm{b}}^4\xi_{\mathrm{b}}\vartheta+\nu_{\mathrm{s}}^2\xi_{\mathrm{b}}\nu_{\mathrm{b}}^2\vartheta\mu_{\mathrm{d}}^3+8\nu_{\mathrm{s}}^2\xi_{\mathrm{b}}\nu_{\mathrm{b}}^2\vartheta\xi_{\mathrm{s}}^2\mu_{\mathrm{d}}+4\xi_{\mathrm{s}}\,\nu_{\mathrm{s}}\nu_{\mathrm{b}}^3\xi_{\mathrm{b}}^2\vartheta^2+4\xi_{\mathrm{s}}\nu_{\mathrm{s}}^3\nu_{\mathrm{b}}\xi_{\mathrm{b}}^2\vartheta^2 \\ & +\xi_{\mathrm{s}}\nu_{\mathrm{s}}\nu_{\mathrm{b}}^3\mu_{\mathrm{d}}^3+6\mu_{\mathrm{d}}^2\nu_{\mathrm{b}}^4\xi_{\mathrm{b}}\vartheta+4\,\nu_{\mathrm{s}}^2\xi_{\mathrm{b}}\nu_{\mathrm{b}}^2\vartheta\xi_{\mathrm{s}}^2+2\xi_{\mathrm{s}}\nu_{\mathrm{s}}\nu_{\mathrm{b}}^3\mu_{\mathrm{d}}^2+\xi_{\mathrm{s}}\nu_{\mathrm{s}}^3\nu_{\mathrm{b}}\mu_{\mathrm{d}}^2+4\mu_{\mathrm{d}}\nu_{\mathrm{b}}^4\xi_{\mathrm{b}}\vartheta \\ & -3\nu_{\mathrm{s}}^2\xi_{\mathrm{b}}\nu_{\mathrm{b}}^2\vartheta\mu_{\mathrm{d}}+\xi_{\mathrm{s}}\nu_{\mathrm{s}}\nu_{\mathrm{b}}^3\mu_{\mathrm{d}}+\xi_{\mathrm{b}}\vartheta\nu_{\mathrm{b}}^4-2\nu_{\mathrm{s}}^2\xi_{\mathrm{b}}\nu_{\mathrm{b}}^2\vartheta+\nu_{\mathrm{s}}^4\xi_{\mathrm{b}}\vartheta)/(2\nu_{\mathrm{s}}^3(4\xi_{\mathrm{b}}^3\vartheta^3\xi_{\mathrm{s}}\nu_{\mathrm{s}}^2\nu_{\mathrm{b}}^2\mu_{\mathrm{d}} \\ & +4\xi_{\mathrm{s}}^2\nu_{\mathrm{s}}\nu_{\mathrm{b}}^3\xi_{\mathrm{b}}^2\vartheta^2\mu_{\mathrm{d}}+4\xi_{\mathrm{b}}^3\vartheta^3\xi_{\mathrm{s}}\nu_{\mathrm{s}}^2\nu_{\mathrm{b}}^2+4\xi_{\mathrm{s}}^2\nu_{\mathrm{s}}\nu_{\mathrm{b}}^3\xi_{\mathrm{b}}^2\vartheta^2+4\nu_{\mathrm{b}}\nu_{\mathrm{s}}^3\xi_{\mathrm{b}}^2\xi_{\mathrm{s}}^2\vartheta^2+\mu_{\mathrm{d}}^2\nu_{\mathrm{b}}^4\xi_{\mathrm{b}}\xi_{\mathrm{s}}\vartheta \\ & +\mu_{\mathrm{d}}\nu_{\mathrm{b}}\nu_{\mathrm{s}}^3\xi_{\mathrm{b}}^2\vartheta^2+4\xi_{\mathrm{b}}\vartheta\xi_{\mathrm{s}}^3\nu_{\mathrm{s}}^2\nu_{\mathrm{b}}^2+2\mu_{\mathrm{d}}\nu_{\mathrm{b}}^4\xi_{\mathrm{b}}\xi_{\mathrm{s}}\vartheta+\xi_{\mathrm{s}}^2\nu_{\mathrm{s}}\nu_{\mathrm{b}}^3\mu_{\mathrm{d}}+\xi_{\mathrm{b}}\xi_{\mathrm{s}}\vartheta\nu_{\mathrm{b}}^4 \\ & -2\xi_{\mathrm{b}}\,\vartheta\xi_{\mathrm{s}}\nu_{\mathrm{s}}^2\nu_{\mathrm{b}}^2+\nu_{\mathrm{s}}^4\xi_{\mathrm{b}}\,\xi_{\mathrm{s}}\vartheta)).\end{aligned} \tag{14}$$

The mathematical expressions to derive the closed-form expression for optimal damping ratio and natural frequency are derived as

$$\frac{\partial\sigma_{u_{\mathrm{s}}^2}}{\partial\xi_{\mathrm{b}}}=0, \quad \frac{\partial\sigma_{u_{\mathrm{s}}^2}}{\partial\nu_{\mathrm{b}}}=0. \tag{15}$$

Equation (14) is substituted into the first expression of Eq. (15), yielding

$$\xi_{\mathrm{b}} = \frac{(\nu_{\mathrm{b}}^2\mu_{\mathrm{d}}^2 + 2\mu_{\mathrm{d}}\nu_{\mathrm{b}}^2 - \mu_{\mathrm{d}}\nu_{\mathrm{s}}^2 + \nu_{\mathrm{b}}^2 - 2\nu_{\mathrm{s}}^2)\xi_{\mathrm{s}}}{2\nu_{\mathrm{b}}\nu_{\mathrm{s}}\vartheta(\mu_{\mathrm{d}}+1)^2}. \tag{16}$$

Equation (16) is substituted into Eq. (14), and the modified version of the standard deviation of displacement is derived as

$$\begin{aligned}
\sigma_{u_{\mathrm{s}}}^2 = {} & (3\mu_{\mathrm{d}}^6\nu_{\mathrm{b}}^6\xi_{\mathrm{s}}^2 + \mu_{\mathrm{d}}^7\nu_{\mathrm{b}}^6 + 18\mu_{\mathrm{d}}^5\nu_{\mathrm{b}}^6\xi_{\mathrm{s}}^2 - \mu_{\mathrm{d}}^5\nu_{\mathrm{b}}^4\nu_{\mathrm{s}}^2\xi_{\mathrm{s}}^2 + 7\mu_{\mathrm{d}}^6\nu_{\mathrm{b}}^6 + 2\mu_{\mathrm{d}}^6\nu_{\mathrm{b}}^4\nu_{\mathrm{s}}^2 + 45\mu_{\mathrm{d}}^4\nu_{\mathrm{b}}^6\xi_{\mathrm{s}}^2 \\
& - 12\mu_{\mathrm{d}}^4\nu_{\mathrm{b}}^4\nu_{\mathrm{s}}^2\xi_{\mathrm{s}}^2 - 3\mu_{\mathrm{d}}^4\nu_{\mathrm{b}}^2\nu_{\mathrm{s}}^4\xi_{\mathrm{s}}^2 + 21\mu_{\mathrm{d}}^5\nu_{\mathrm{b}}^6 + 6\mu_{\mathrm{d}}^5\nu_{\mathrm{b}}^4\nu_{\mathrm{s}}^2 + \mu_{\mathrm{d}}^5\nu_{\mathrm{b}}^2\nu_{\mathrm{s}}^4 + 60\mu_{\mathrm{d}}^3\nu_{\mathrm{b}}^6\xi_{\mathrm{s}}^2 \\
& - 38\mu_{\mathrm{d}}^3\nu_{\mathrm{b}}^4\nu_{\mathrm{s}}^2\xi_{\mathrm{s}}^2 - 10\mu_{\mathrm{d}}^3\nu_{\mathrm{b}}^2\nu_{\mathrm{s}}^4\xi_{\mathrm{s}}^2 + \mu_{\mathrm{d}}^3\nu_{\mathrm{s}}^6\xi_{\mathrm{s}}^2 + 35\mu_{\mathrm{d}}^4\nu_{\mathrm{b}}^6 + 3\mu_{\mathrm{d}}^4\nu_{\mathrm{b}}^2\nu_{\mathrm{s}}^4 + 45\mu_{\mathrm{d}}^2\nu_{\mathrm{b}}^6\xi_{\mathrm{s}}^2 \\
& - 52\mu_{\mathrm{d}}^2\nu_{\mathrm{b}}^4\nu_{\mathrm{s}}^2\xi_{\mathrm{s}}^2 - 7\mu_{\mathrm{d}}^2\nu_{\mathrm{b}}^2\nu_{\mathrm{s}}^4\xi_{\mathrm{s}}^2 + 4\mu_{\mathrm{d}}^2\nu_{\mathrm{s}}^6\xi_{\mathrm{s}}^2 + 35\mu_{\mathrm{d}}^3\nu_{\mathrm{b}}^6 - 20\mu_{\mathrm{d}}^3\nu_{\mathrm{b}}^4\nu_{\mathrm{s}}^2 + 8\mu_{\mathrm{d}}^3\nu_{\mathrm{b}}^2\nu_{\mathrm{s}}^4 \\
& + 18\mu_{\mathrm{d}}\nu_{\mathrm{b}}^6\xi_{\mathrm{s}}^2 - 33\mu_{\mathrm{d}}\nu_{\mathrm{b}}^4\nu_{\mathrm{s}}^2\xi_{\mathrm{s}}^2 + 4\mu_{\mathrm{d}}\nu_{\mathrm{b}}^2\nu_{\mathrm{s}}^4\xi_{\mathrm{s}}^2 + 4\mu_{\mathrm{d}}\nu_{\mathrm{s}}^6\xi_{\mathrm{s}}^2 + 21\mu_{\mathrm{d}}^2\nu_{\mathrm{b}}^6 - 30\mu_{\mathrm{d}}^2\nu_{\mathrm{b}}^4\nu_{\mathrm{s}}^2 \\
& + 16\mu_{\mathrm{d}}^2\nu_{\mathrm{b}}^2\nu_{\mathrm{s}}^4 - \mu_{\mathrm{d}}^2\nu_{\mathrm{s}}^6 + 3\nu_{\mathrm{b}}^6\xi_{\mathrm{s}}^2 - 8\nu_{\mathrm{b}}^4\nu_{\mathrm{s}}^2\xi_{\mathrm{s}}^2 + 4\nu_{\mathrm{b}}^2\nu_{\mathrm{s}}^4\xi_{\mathrm{s}}^2 + 7\mu_{\mathrm{d}}\nu_{\mathrm{b}}^6 - 18\mu_{\mathrm{d}}\nu_{\mathrm{b}}^4\nu_{\mathrm{s}}^2 \\
& + 15\mu_{\mathrm{d}}\nu_{\mathrm{b}}^2\nu_{\mathrm{s}}^4 - 3\mu_{\mathrm{d}}\nu_{\mathrm{s}}^6 + \nu_{\mathrm{b}}^6 - 4\nu_{\mathrm{b}}^4\nu_{\mathrm{s}}^2 + 5\nu_{\mathrm{b}}^2\nu_{\mathrm{s}}^4 - 2\nu_{\mathrm{s}}^6)\pi S_0(\mu_{\mathrm{d}}+1)^2 \\
& /(\nu_{\mathrm{s}}^3(6\mu_{\mathrm{d}}^6\nu_{\mathrm{b}}^6\xi_{\mathrm{s}}^2 + 2\mu_{\mathrm{d}}^7\nu_{\mathrm{b}}^6 + 36\mu_{\mathrm{d}}^5\nu_{\mathrm{b}}^6\xi_{\mathrm{s}}^2 - 2\mu_{\mathrm{d}}^5\nu_{\mathrm{b}}^4\nu_{\mathrm{s}}^2\xi_{\mathrm{s}}^2 + 14\mu_{\mathrm{d}}^6\nu_{\mathrm{b}}^6 + 3\mu_{\mathrm{d}}^6\nu_{\mathrm{b}}^4\nu_{\mathrm{s}}^2 \\
& + 90\mu_{\mathrm{d}}^4\nu_{\mathrm{b}}^6\xi_{\mathrm{s}}^2 - 24\mu_{\mathrm{d}}^4\nu_{\mathrm{b}}^4\nu_{\mathrm{s}}^2\xi_{\mathrm{s}}^2 - 6\mu_{\mathrm{d}}^4\nu_{\mathrm{b}}^2\nu_{\mathrm{s}}^4\xi_{\mathrm{s}}^2 + 42\mu_{\mathrm{d}}^5\nu_{\mathrm{b}}^6 + 7\mu_{\mathrm{d}}^5\nu_{\mathrm{b}}^4\nu_{\mathrm{s}}^2 + 120\mu_{\mathrm{d}}^3\nu_{\mathrm{b}}^6\xi_{\mathrm{s}}^2 \\
& - 76\mu_{\mathrm{d}}^3\nu_{\mathrm{b}}^4\nu_{\mathrm{s}}^2\xi_{\mathrm{s}}^2 - 20\mu_{\mathrm{d}}^3\nu_{\mathrm{b}}^2\nu_{\mathrm{s}}^4\xi_{\mathrm{s}}^2 + 2\mu_{\mathrm{d}}^3\nu_{\mathrm{s}}^6\xi_{\mathrm{s}}^2 + 70\mu_{\mathrm{d}}^4\nu_{\mathrm{b}}^6 - 10\mu_{\mathrm{d}}^4\nu_{\mathrm{b}}^4\nu_{\mathrm{s}}^2 + 4\mu_{\mathrm{d}}^4\nu_{\mathrm{b}}^2\nu_{\mathrm{s}}^4 \\
& - \mu_{\mathrm{d}}^4\nu_{\mathrm{s}}^6 + 90\mu_{\mathrm{d}}^2\nu_{\mathrm{b}}^6\xi_{\mathrm{s}}^2 - 104\mu_{\mathrm{d}}^2\nu_{\mathrm{b}}^4\nu_{\mathrm{s}}^2\xi_{\mathrm{s}}^2 - 14\mu_{\mathrm{d}}^2\nu_{\mathrm{b}}^2\nu_{\mathrm{s}}^4\xi_{\mathrm{s}}^2 + 8\mu_{\mathrm{d}}^2\nu_{\mathrm{s}}^6\xi_{\mathrm{s}}^2 + 70\mu_{\mathrm{d}}^3\nu_{\mathrm{b}}^6 \\
& - 50\mu_{\mathrm{d}}^3\nu_{\mathrm{b}}^4\nu_{\mathrm{s}}^2 + 22\mu_{\mathrm{d}}^3\nu_{\mathrm{b}}^2\nu_{\mathrm{s}}^4 - 5\mu_{\mathrm{d}}^3\nu_{\mathrm{s}}^6 + 36\mu_{\mathrm{d}}\nu_{\mathrm{b}}^6\xi_{\mathrm{s}}^2 - 66\mu_{\mathrm{d}}\nu_{\mathrm{b}}^4\nu_{\mathrm{s}}^2\xi_{\mathrm{s}}^2 + 8\mu_{\mathrm{d}}\nu_{\mathrm{b}}^2\nu_{\mathrm{s}}^4\xi_{\mathrm{s}}^2 \\
& + 8\mu_{\mathrm{d}}\nu_{\mathrm{s}}^6\xi_{\mathrm{s}}^2 + 42\mu_{\mathrm{d}}^2\nu_{\mathrm{b}}^6 - 65\mu_{\mathrm{d}}^2\nu_{\mathrm{b}}^4\nu_{\mathrm{s}}^2 + 42\mu_{\mathrm{d}}^2\nu_{\mathrm{b}}^2\nu_{\mathrm{s}}^4 - 10\mu_{\mathrm{d}}^2\nu_{\mathrm{s}}^6 + 6\nu_{\mathrm{b}}^6\xi_{\mathrm{s}}^2 \\
& - 16\nu_{\mathrm{b}}^4\nu_{\mathrm{s}}^2\xi_{\mathrm{s}}^2 + 8\nu_{\mathrm{b}}^2\nu_{\mathrm{s}}^4\xi_{\mathrm{s}}^2 + 14\mu_{\mathrm{d}}\nu_{\mathrm{b}}^6 - 37\mu_{\mathrm{d}}\nu_{\mathrm{b}}^4\nu_{\mathrm{s}}^2 + 34\mu_{\mathrm{d}}\nu_{\mathrm{b}}^2\nu_{\mathrm{s}}^4 - 10\mu_{\mathrm{d}}\nu_{\mathrm{s}}^6 \\
& + 2\nu_{\mathrm{b}}^6 - 8\nu_{\mathrm{b}}^4\nu_{\mathrm{s}}^2 + 10\nu_{\mathrm{b}}^2\nu_{\mathrm{s}}^4 - 4\nu_{\mathrm{s}}^6)\xi_{\mathrm{s}}).
\end{aligned} \tag{17}$$

Equation (17) is substituted into the second expression of Eq. (15). Accordingly, the closed-form expression for the optimal natural frequency of the damper is derived as

$$(\nu_{\mathrm{b}})_{\mathrm{opt}} = \sqrt{\frac{(2-\mu_{\mathrm{d}})\nu_{\mathrm{s}}^2}{(\mu_{\mathrm{d}}+1)^2}}. \tag{18}$$

Equation (18) is substituted into Eq. (16). The optimal damping ratio of the damper is derived as

$$(\xi_{\mathrm{b}})_{\mathrm{opt}} = \frac{\mu_{\mathrm{d}}\xi_{\mathrm{s}}}{\vartheta(\mu_{\mathrm{d}}+1)^2}\frac{1}{\sqrt{\frac{(2-\mu_{\mathrm{d}})}{(\mu_{\mathrm{d}}+1)^2}}}. \tag{19}$$

By altering the damper's mass ratio, the ideal frequency ratio can be visually shown. In Fig. 2, the graphical representation is displayed. Utilizing Eq. (18), this graph is produced. When the mass ratio of the isolator grows, the frequency ratio progressively rises. κ_{b} defines the frequency ratio of the absorber. Concurrently, Eq. (19) is also used to build this kind of parametric graph for the optimal damping ratio of the dampers. As a result, Fig. 3 displays the variations in each damper's ideal damping ratio. The numerical values of the damping ratio undergo rapid changes when the structural damping ratio is included in the closed-form expression. In particular, the damper's damping ratio degrades rapidly, which raises the possibility of higher production costs. In fact, to achieve the robust performance from H_2 optimized design parameters, i.e., ξ_{b} and κ_{b}, including the damping ratio of the structure, i.e., $\xi_{\mathrm{s}} \neq 0$, and to properly tune the damper with the primary structure, the damping ratio of the structure needs

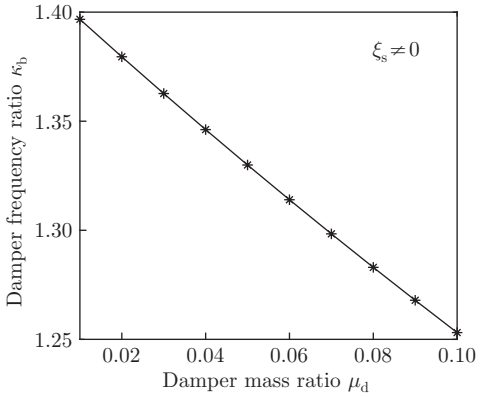

Fig. 2 Variations in the optimal frequency ratio of the dampers as a function of the mass ratio of the damper

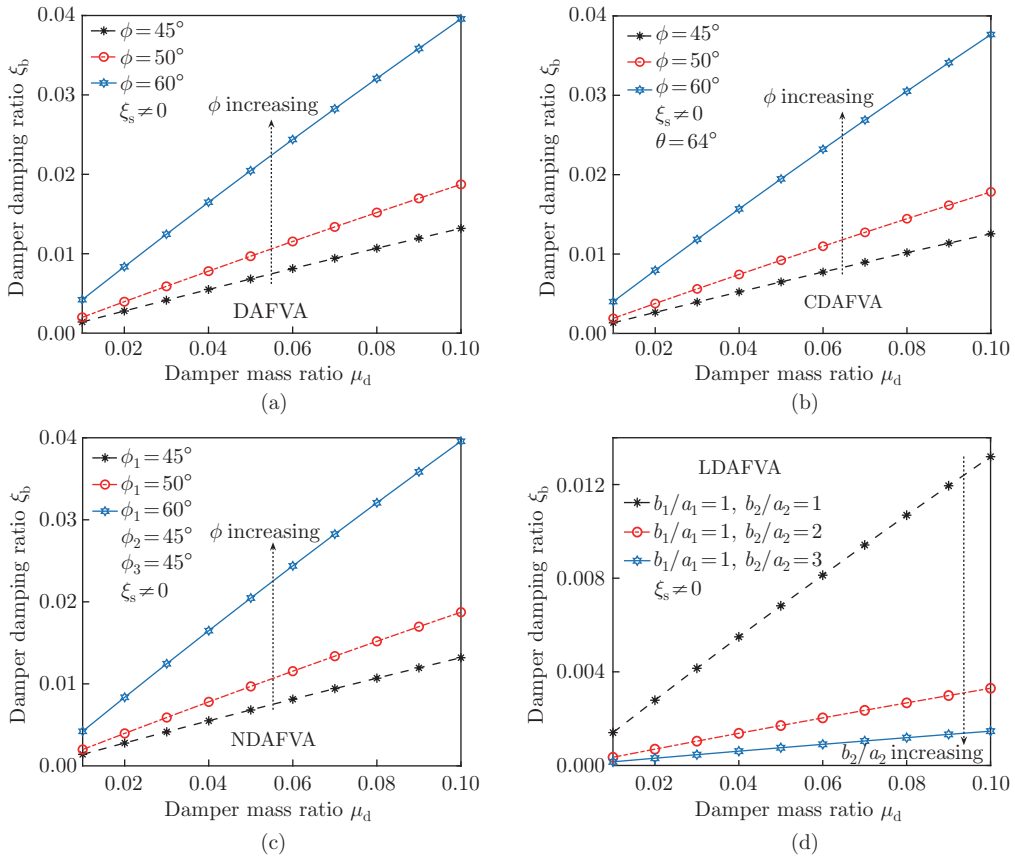

Fig. 3 Variations in the optimal damping ratio of the (a) DAFVA, (b) CDAFVA, (c) NDAFVA, and (d) LDAFVA as a function of the mass ratio of the damper (color online)

to be set to 0.2. This value is slightly higher and may increase the manufacturing cost. ξ_s has a value between 0.05 and 0.2. It demonstrates that for all DAFVAs, the damping ratios are progressively rising. For these specific graphs, the damping of the SDOF system is taken to be 0.2, i.e., $\xi_s = 0.2$. The damping ratio variations for DAFVAs, CDAFVAs, NDAFVAs, and

LDAFVAs with respect to the isolator mass ratio are shown in Figs. 3(a), 3(b), 3(c), and 3(d). The damper damping ratio is a function of the variable damper mass ratio. In the case of the DAFVAs, the damping ratio progressively rises with increasing damping amplifier angle and falls with increasing isolator mass ratio. The CDAFVAs with the primary damping amplifier angle exhibit the same properties. The robust value of the secondary damping amplifier angle is evaluated as 64°. Furthermore, the NDAFVA shares the same physical properties of the damping ratio as DAFVAs and CDAFVAs. The damping ratio of the TMD is influenced by three amplifier angles: primary, secondary, and tertiary. For this graph, the secondary and tertiary angles remain unchanged. Regarding applying the minimal lever arm ratio, the LDAFVA's characteristics differ slightly from those of the other three vibration absorbers. The value of b_1/a_1 is maintained constant, i.e., $b_1/a_1 = 1.0$, to preserve the design's simplicity. b_2/a_2 has a value that ranges from 1 to 3. A greater value of the b_2/a_2 ratio dramatically reduces the ideal damping ratio, making it unsuitable for use as a TMD. To obtain a strong vibration reduction capacity from the LDAFVA, a lower value of b_2/a_2 is necessary for its ideal design.

2.1.2 Derivation of the optimal design parameters by considering $\xi_\mathrm{s} = 0$

For this particular optimization study, the primary structure's damping is now regarded as zero, denoted by the expression $\xi_\mathrm{s} = 0$. Both the closed-form formula for the standard deviation and the optimum design parameters are undergoing changes at the same time. Therefore, in order to achieve the outcomes that are wanted from this analysis, the values of ξ_s in Eq. (11) and Eq. (13) are taken into consideration to be zero. In addition, the denominator of Eq. (13) is a polynomial equation of the fourth order. With the use of the H_2 optimization approach for random white noise excitation, the standard deviation for the displacement of the SDOF system is determined as follows:

$$\sigma^2_{u_\mathrm{s}} = S_0\pi(4\mu_\mathrm{d}^3\nu_\mathrm{b}^2\nu_\mathrm{s}^2\xi_\mathrm{b}^2\vartheta^2 + 12\mu_\mathrm{d}^2\nu_\mathrm{b}^2\nu_\mathrm{s}^2\xi_\mathrm{b}^2\vartheta^2 + 12\mu_\mathrm{d}\nu_\mathrm{b}^2\nu_\mathrm{s}^2\xi_\mathrm{b}^2\vartheta^2 + \mu_\mathrm{d}^4\nu_\mathrm{b}^4 + 4\nu_\mathrm{b}^2\nu_\mathrm{s}^2\xi_\mathrm{b}^2\vartheta^2 + 4\mu_\mathrm{d}^3\nu_\mathrm{b}^4 + \mu_\mathrm{d}^3\nu_\mathrm{b}^2\nu_\mathrm{s}^2 + 6\mu_\mathrm{d}^2\nu_\mathrm{b}^4 + 4\mu_\mathrm{d}\nu_\mathrm{b}^4 - 3\mu_\mathrm{d}\nu_\mathrm{b}^2\nu_\mathrm{s}^2 + \nu_\mathrm{b}^4 - 2\nu_\mathrm{b}^2\nu_\mathrm{s}^2 + \nu_\mathrm{s}^4)/(2\nu_\mathrm{b}\xi_\mathrm{b}\vartheta\mu_\mathrm{d}\nu_\mathrm{s}^6). \tag{20}$$

Equation (20) is partially differentiated with respect to the damping ratio and natural frequency of the damper to obtain their optimal values, and the corresponding mathematical expression is derived as

$$\frac{\partial\sigma^2_{u_\mathrm{s}}}{\partial\xi_\mathrm{b}} = 0, \quad \frac{\partial\sigma^2_{u_\mathrm{s}}}{\partial\nu_\mathrm{b}} = 0. \tag{21}$$

Equation (20) is substituted into the first expression of Eq. (21) and the damping ratio of the damper is derived as

$$\xi_\mathrm{b} = \sqrt{(\mu_\mathrm{d}+1)(\mu_\mathrm{d}^4\nu_\mathrm{b}^4 + 4\mu_\mathrm{d}^3\nu_\mathrm{b}^4 + \mu_\mathrm{d}^3\nu_\mathrm{b}^2\nu_\mathrm{s}^2 + 6\mu_\mathrm{d}^2\nu_\mathrm{b}^4 + 4\mu_\mathrm{d}\nu_\mathrm{b}^4 - 3\mu_\mathrm{d}\nu_\mathrm{b}^2\nu_\mathrm{s}^2 + \nu_\mathrm{b}^4 - 2\nu_\mathrm{b}^2\nu_\mathrm{s}^2 + \nu_\mathrm{s}^4)} /(2(\mu_\mathrm{d}+1)^2\vartheta\nu_\mathrm{s}\nu_\mathrm{b}). \tag{22}$$

Equation (22) is substituted into Eq. (20). Accordingly, the modified version of Eq. (20) is derived, which has only the natural frequency of the damper in terms of optimal governing system parameters.

$$\sigma^2_{u_\mathrm{s}} = \frac{2((\mu_\mathrm{d}+1)^4\nu_\mathrm{b}^4 + \nu_\mathrm{s}^2(\mu_\mathrm{d}-2)(\mu_\mathrm{d}+1)^2\nu_\mathrm{b}^2 + \nu_\mathrm{s}^4)S_0(\mu_\mathrm{d}+1)^2\pi}{\sqrt{(\mu_\mathrm{d}+1)((\mu_\mathrm{d}+1)^4\nu_\mathrm{b}^4 + \nu_\mathrm{s}^2(\mu_\mathrm{d}-2)(\mu_\mathrm{d}+1)^2\nu_\mathrm{b}^2 + \nu_\mathrm{s}^4)}\nu_\mathrm{s}^5\mu_\mathrm{d}}. \tag{23}$$

Equation (23) is substituted into the second expression of Eq. (21). As a result, the closed-form expression for the optimal frequency of the damper is determined as

$$(\nu_\mathrm{b})_\mathrm{opt} = \nu_\mathrm{s}\sqrt{\frac{2-\mu_\mathrm{d}}{2\mu_\mathrm{d}^2 + 4\mu_\mathrm{d} + 2}}. \tag{24}$$

Equation (24) is substituted into Eq. (22), and the optimal closed-form solutions for the damping ratio of the damper are derived as

$$(\xi_{\mathrm{b}})_{\mathrm{opt}} = \frac{\sqrt{\mu_{\mathrm{d}}(\mu_{\mathrm{d}}+1)(4-\mu_{\mathrm{d}})}}{2\vartheta(\mu_{\mathrm{d}}+1)\sqrt{4-2\mu_{\mathrm{d}}}}. \tag{25}$$

The standard deviation of the velocity of the absorber is derived as

$$\sigma^2_{\dot{u}_{\mathrm{d}}} = \frac{S_0\pi(\mu_{\mathrm{d}}+1)}{2\nu_{\mathrm{b}}\xi_{\mathrm{b}}\vartheta\mu_{\mathrm{d}}}. \tag{26}$$

The optimal frequency ratio can be found by treating the primary structure's damping ratio as zero. Compared with the prior one, where the damping of the fundamental structure is not regarded as zero, it now has different physical features. Figure 4 displays a graph that is created using Eq. (24) to pinpoint the precise changes. κ_{b} defines the frequency ratio of the absorber. This means that each damper's damping ratio has the same physical properties as those displayed in Fig. 5. The numerical values of the damping ratio undergo significant modifications when the structural damping ratio is not included in the closed-form expression. A sufficient damping ratio can be achieved for these suggested dampers without using the greater value of the damping ratio of the primary structure. If the primary structure's damping ratio, or $\xi_{\mathrm{s}} = 0$, is not considered when doing the H_2 optimization procedure, it will be easy to attain robust performance from the suggested dampers. Figure 6 illustrates the variations in the ideal damping ratio values for the isolators when non-zero and zero structure damping are considered. In particular, the damper's damping ratio degrades rapidly, which raises the possibility of higher production costs when the primary structure's damping ratio is considered during the optimization procedure. To achieve the robust performance from H_2 optimized design parameters, i.e., ξ_{b} and κ_{b}, including the damping ratio of the structure, i.e., $\xi_{\mathrm{s}} \neq 0$, and to properly tune the damper with the primary structure, the damping ratio of the structure needs to be set to 0.2. This value is higher and may increase the manufacturing cost. The damping of the SDOF system is considered 0, i.e., $\xi_{\mathrm{s}} = 0$ (see Fig. 5). The damping ratio variations for DAFVAs, CDAFVAs, NDAFVAs, and LDAFVAs with respect to the damper mass ratio are specifically displayed in Figs. 5(a), 5(b), 5(c), and 5(d). The damper damping ratio is a function of the variable damper mass ratio. For the standard mass damper with a tuned damping amplifier, the damping ratio progressively rises with the damping amplifier angle and falls with each increment of the damper mass ratio. The CDAFVAs with the primary damping amplifier angle exhibit the same properties. The value of the secondary damping amplifier angle

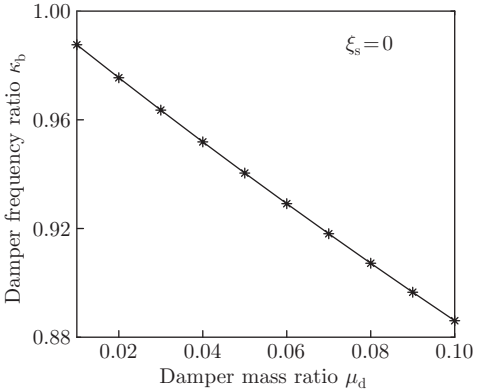

Fig. 4 Variations in the optimal frequency ratio of the dampers as a function of the mass ratio of the damper

is 64°. In addition, like ordinary and compound vibration absorbers, the physical characteristics of the damping ratio of the NDAFVAs are the same. Three amplifier angles affect the damping ratio of the TMD, i.e., primary, secondary, and tertiary. The secondary and tertiary angles are kept constant for this graph. Compared with the other three dampers, the characteristics of the LDAFVAs are slightly different in terms of applying the minimum lever arm ratio. To maintain the simplicity in the design, the value of b_1/a_1 is kept constant, i.e., $b_1/a_1 = 1.0$. The value of b_2/a_2 varies from 1 to 3. The optimal damping ratio is drastically lowered for a higher value of the b_2/a_2 ratio, which is unsuitable for these novel dampers. Therefore, a lower value of b_2/a_2 is required to optimally design the LDAFVAs to achieve a robust vibration reduction capacity from it.

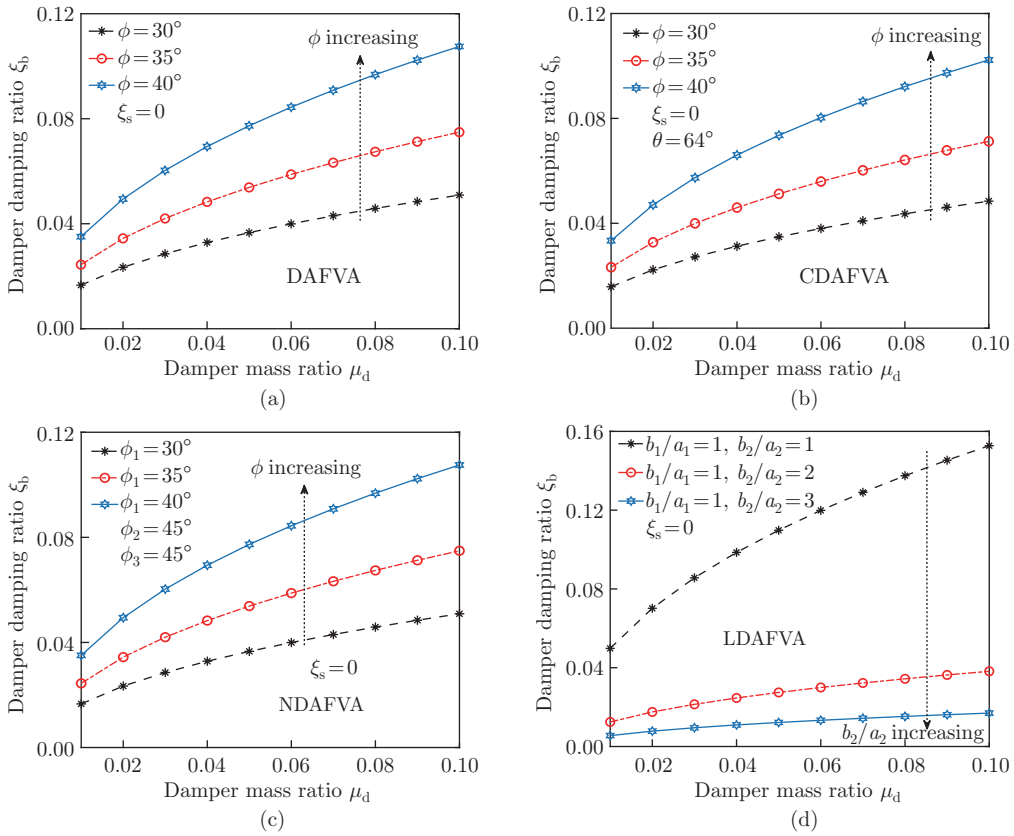

Fig. 5 Variations in the optimal damping ratio of the (a) DAFVA, (b) CDAFVA, (c) NDAFVA, and (d) LDAFVA as a function of the mass ratio of the damper (color online)

2.2 H_∞ optimization

Now, the controlled SDOF system is subjected to harmonic excitation. Therefore, H_∞ optimization is applicable. Equation (10) is non-dimensionalized in order to apply this optimization method,

$$\begin{pmatrix} 2\mathrm{i}\kappa\xi_s + 1 - \kappa^2 & -2\mathrm{i}\mu_d\kappa_b\kappa\xi_b\vartheta - \mu_d\kappa_b^2 \\ -\mu_d\kappa^2 & 2\mathrm{i}\mu_d\kappa_b\kappa\xi_b\vartheta + \mu_d\kappa_b^2 - \mu_d\kappa^2 \end{pmatrix} \begin{pmatrix} U_s \\ U_d \end{pmatrix} = -\begin{pmatrix} 1 \\ \mu_d \end{pmatrix} \frac{U_g}{\nu_s^2}. \tag{27}$$

$\kappa\,(=\omega/\nu_s)$ defines the excitation frequency ratio. The displacement of the SDOF system is derived as

$$\tilde{H}_s = \left(\frac{U_s}{U_g}\right)\nu_s^2 = \frac{\mu_d\kappa_b^2 - \kappa^2 + \kappa_b^2 + \mathrm{i}(2\mu_d\kappa_b\kappa\xi_b\vartheta + 2\kappa\xi_b\kappa_b\vartheta)}{\tilde{\Delta}_f}. \tag{28}$$

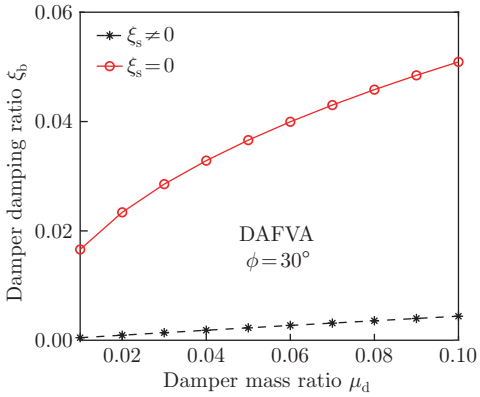

Fig. 6 Variations in the optimal damping ratio of the DAFVAs as a function of the mass ratio of the damper may be observed when the damping ratio of the primary structure is considered to be non-zero and zero, i.e., $\xi_s \neq 0$ and $\xi_s = 0$. Equations (19) and (25) are applied to obtain this graph. The damping ratio of the primary structure is 0.20, i.e., $\xi_s = 0.20$, for Eq. (19). The values of the damping amplifier angles for both optimal closed-form solutions are considered the same, i.e., $\phi = 30^o$, to maintain a fair comparison between them and to locate the exact changes in their physical characteristics. The transition between the primary structure's damping ratio and the optimal damping ratio of the TMD for its robust design, as well as the requirement for its presence in the optimal closed-form solutions, is evaluated using this graph (color online)

The displacement of the damper is derived as

$$\tilde{H}_d = \left(\frac{U_d}{U_g}\right)\nu_s^2 = \frac{2i\kappa\xi_s + 1}{\tilde{\Delta}_f}. \tag{29}$$

The denominator of Eqs. (28) and (29) is obtained as

$$\begin{aligned}\tilde{\Delta}_f = {} & 4\kappa^2\xi_b\xi_s\kappa_b\vartheta + \kappa^2\mu_d\kappa_b^2 - \kappa^4 + \kappa^2\kappa_b^2 + \kappa^2 - \kappa_b^2 \\ & + i(2\kappa^3\mu_d\xi_b\kappa_b\vartheta + 2\kappa^3\xi_b\kappa_b\vartheta + 2\kappa^3\xi_s - 2\kappa\xi_b\kappa_b\vartheta - 2\kappa\xi_s\kappa_b^2).\end{aligned} \tag{30}$$

The resultant of Eqs. (28) and (30) is written as

$$|\tilde{H}_s| = \sqrt{\frac{A_1^2 + \xi_b^2 B_1^2}{C_1^2 + \xi_b^2 D_1^2}}. \tag{31}$$

The above equation formation is only achieved according to the H_∞ optimization method/fixed point theory when the damping ratio of the primary structure (i.e., SDOF system) is considered zero, i.e., $\xi_s = 0$. After applying this condition to Eqs. (28) and (30), the closed-form expressions for A_1, B_1, C_1, and D_1 are derived as

$$\begin{cases} A_1 = \mu_d\kappa_b^2 - \kappa^2 + \kappa_b^2, \quad B_1 = 2\kappa\mu_d\kappa_b\vartheta + 2\kappa\kappa_b\vartheta, \\ C_1 = \kappa^2\mu_d\kappa_b^2 - \kappa^4 + \kappa^2\kappa_b^2 + \kappa^2 - \kappa_b^2, \quad D_1 = 2\kappa^3\mu_d\kappa_b\vartheta + 2\kappa^3\kappa_b\vartheta - 2\kappa\kappa_b\vartheta. \end{cases} \tag{32}$$

Two constraints are derived from Eq. (31) for deriving the optimal closed-form solutions for governing system parameters of the damper.

$$\left|\frac{A_1}{B_1}\right|_{\kappa_j} = \left|\frac{C_1}{D_1}\right|_{\kappa_j}, \quad \left|\frac{B_1}{D_1}\right|_{\kappa_1} = \left|\frac{B_1}{D_1}\right|_{\kappa_2}. \tag{33}$$

Equation (32) is substituted into the first expression of Eq. (33), yielding

$$(2\mu_{\mathrm{d}}+2)\kappa^4+(-2\mu_{\mathrm{d}}^2\kappa_{\mathrm{b}}^2-4\mu_{\mathrm{d}}\kappa_{\mathrm{b}}^2-2\kappa_{\mathrm{b}}^2-\mu_{\mathrm{d}}-2)\kappa^2+2\mu_{\mathrm{d}}\kappa_{\mathrm{b}}^2+2\kappa_{\mathrm{b}}^2=0. \tag{34}$$

Equation (34) is written as

$$\kappa^4+(-\kappa_1^2-\kappa_2^2)\kappa^2+\kappa_1^2\kappa_2^2=0. \tag{35}$$

By comparing Eq. (34) with Eq. (35), the summation of the two roots, i.e., $\kappa_{1,2}^2$, is derived as

$$\kappa_1^2+\kappa_2^2=\frac{2(\mu_{\mathrm{d}}+1)^2\kappa_{\mathrm{b}}^2+\mu_{\mathrm{d}}+2}{2\mu_{\mathrm{d}}+2}. \tag{36}$$

Equation (32) is substituted into the second expression of Eq. (33), yielding

$$\kappa_1^2+\kappa_2^2=\frac{2}{1+\mu_{\mathrm{d}}}. \tag{37}$$

Equations (36) and (37) are equated to obtain the closed-form expression for the optimal natural frequency of the damper and expressed as

$$(\kappa_{\mathrm{b}})_{\mathrm{opt}}=\sqrt{\frac{2-\mu_{\mathrm{d}}}{2\mu_{\mathrm{d}}^2+4\mu_{\mathrm{d}}+2}}. \tag{38}$$

The value of each root, i.e., κ_1^2 and κ_2^2, is derived using Eq. (34) and Eq. (37).

$$\kappa_{1,2}^2=\frac{1\pm\sqrt{1-\mu_{\mathrm{d}}^2\kappa_{\mathrm{b}}^2-2\mu_{\mathrm{d}}\kappa_{\mathrm{b}}^2-\kappa_{\mathrm{b}}^2}}{\mu_{\mathrm{d}}+1}. \tag{39}$$

The closed-form expression for the optimal damping ratio of the damper is obtained by forming an analytical equation,

$$\frac{\partial|\tilde{H}_{\mathrm{s}}(\kappa)|^2}{\partial\kappa^2}\Big|_{\kappa_{1,2}^2}=0,\quad (\xi_{\mathrm{b}})_{\mathrm{opt}}=\sqrt{\frac{\xi_{\mathrm{b1}}^2+\xi_{\mathrm{b2}}^2}{2}}. \tag{40}$$

The square of Eq. (31) is partially substituted by κ^2. Accordingly, the closed-form expression for the optimal damping ratio of the damper is derived as

$$P_1\xi_{\mathrm{b}}^4+P_2\xi_{\mathrm{b}}^2+P_3=0,\quad (\xi_{\mathrm{b1,b2}})_{\kappa_{1,2}^2}^2=\frac{-P_2+\sqrt{-4P_1P_3+P_2^2}}{2P_1}. \tag{41}$$

The closed-form expressions for P_1, P_2, and P_3 are derived as

$$\begin{cases}
P_1=-32\kappa_{1,2}^4\kappa_{\mathrm{b}}^4\vartheta^4(\mu_{\mathrm{d}}+1)^3(\kappa_{1,2}^2\mu_{\mathrm{d}}+\kappa_{1,2}^2-1),\\
P_2=(-16\mu_{\mathrm{d}}^2\kappa_{\mathrm{b}}^2\vartheta^2-32\mu_{\mathrm{d}}\kappa_{\mathrm{b}}^2\vartheta^2-16\kappa_{\mathrm{b}}^2\vartheta^2)\kappa_{1,2}^8+(32\mu_{\mathrm{d}}^3\kappa_{\mathrm{b}}^4\vartheta^2+96\mu_{\mathrm{d}}^2\kappa_{\mathrm{b}}^4\vartheta^2\\
\quad+96\mu_{\mathrm{d}}\kappa_{\mathrm{b}}^4\vartheta^2+16\mu_{\mathrm{d}}^2\kappa_{\mathrm{b}}^2\vartheta^2+32\kappa_{\mathrm{b}}^4\vartheta^2+32\mu_{\mathrm{d}}\kappa_{\mathrm{b}}^2\vartheta^2+16\kappa_{\mathrm{b}}^2\vartheta^2)\kappa_{1,2}^6\\
\quad+(-16\mu_{\mathrm{d}}^4\kappa_{\mathrm{b}}^6\vartheta^2-64\mu_{\mathrm{d}}^3\kappa_{\mathrm{b}}^6\vartheta^2-96\mu_{\mathrm{d}}^2\kappa_{\mathrm{b}}^6\vartheta^2-8\mu_{\mathrm{d}}^3\kappa_{\mathrm{b}}^4\vartheta^2-64\mu_{\mathrm{d}}\kappa_{\mathrm{b}}^6\vartheta^2-48\mu_{\mathrm{d}}^2\kappa_{\mathrm{b}}^4\vartheta^2\\
\quad-16\kappa_{\mathrm{b}}^6\vartheta^2-72\mu_{\mathrm{d}}\kappa_{\mathrm{b}}^4\vartheta^2-4\mu_{\mathrm{d}}^2\kappa_{\mathrm{b}}^2\vartheta^2-32\kappa_{\mathrm{b}}^4\vartheta^2-8\mu_{\mathrm{d}}\kappa_{\mathrm{b}}^2\vartheta^2)\kappa_{1,2}^4+(16\mu_{\mathrm{d}}^3\kappa_{\mathrm{b}}^6\vartheta^2\\
\quad+48\mu_{\mathrm{d}}^2\kappa_{\mathrm{b}}^6\vartheta^2+48\mu_{\mathrm{d}}\kappa_{\mathrm{b}}^6\vartheta^2+16\kappa_{\mathrm{b}}^6\vartheta^2)\kappa_{1,2}^2,\\
P_3=(-2(1+(-1-\mu_{\mathrm{d}})\kappa_{1,2}^2)\kappa_{\mathrm{b}}^2-2\kappa_{1,2}^4+2\kappa_{1,2}^2)((-1-\mu_{\mathrm{d}})\kappa_{\mathrm{b}}^2+\kappa_{1,2}^2)\\
\quad((\mu_{\mathrm{d}}+1)^2\kappa_{\mathrm{b}}^4+((-2\mu_{\mathrm{d}}-2)\kappa_{1,2}^2+\mu_{\mathrm{d}})\kappa_{\mathrm{b}}^2+\kappa_{1,2}^4).
\end{cases} \tag{42}$$

The H_∞ optimization technique is used to obtain the frequency ratio variations. These variations are shown in Fig. 7, which is derived using Eq. (38). This graph indicates that the ideal frequency ratio drops as the damper mass ratio increases, giving the damper more flexibility while maintaining a high enough load-bearing capability during vibration. This kind of parametric graph is also produced concurrently with the use of Eq. (41) and Eq. (42) for the evaluation of the optimal damping ratio of the damper. As a result, Fig. 8 displays the variations in each damper's ideal damping ratio. Figures 8(a)–8(d) illustrate the variations in the damping ratio for the DAFVAs, CDAFVAs, NDAFVAs, and LDAFVAs in relation to the damper mass ratio. The variable damper mass ratio determines the damper's damping ratio. The damping ratio gradually increases with increasing damping amplifier angle and decreases with increasing isolator mass ratio in the case of the DAFVAs. The same characteristics are shown by the CDAFVAs with the primary damping amplifier angle. 64° is the value of the secondary damping amplifier angle. Furthermore, the physical characteristics of the damping ratio of ordinary and compound vibration absorbers are also shared by the NDAFVAs. The primary, secondary, and tertiary amplifier angles have an impact on the damper's damping ratio. The tertiary and secondary angles on this graph remain constant. The features of the LDAFVAs are marginally different from those of the other three dampers when it comes to applying the minimal lever arm ratio. To keep the design simple, the value of b_1/a_1 is kept constant, that is, $b_1/a_1 = 1.0$. The number for b_2/a_2 can be between 1 and 3. An increase in the b_2/a_2 ratio leads to a significant decrease in the optimal damping ratio, rendering it unfit for application as a damper. A lower value of b_2/a_2 is required for the ideal design of the LDAFVAs in order to achieve a great vibration reduction capability.

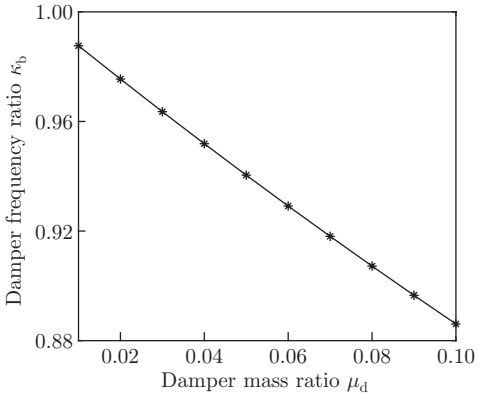

Fig. 7 Variations in the optimal frequency ratio of the dampers as a function of the mass ratio of the damper

3 Dynamic response evaluation

The newly developed damping-amplifier base isolators and vibration absorbers are applied to the SDOF systems to achieve their vibration reduction performance. The governing system parameters are considered the same for all controlled SDOF systems. The harmonic excitation is applied at the base of the controlled structures. As a result, the dynamic responses are generated by the controlled structures. The detailed analysis of dynamic response evaluation is illustrated in the following subsections.

3.1 Novel vibration absorbers installed in the SDOF systems

Every suggested mass damper with a tuned damping amplifier is applied at the top of the systems with an SDOF that is excited harmonically at the base. To find out how well the damper is reducing the vibration of the SDOF systems, the H_2 optimized vibration absorbers

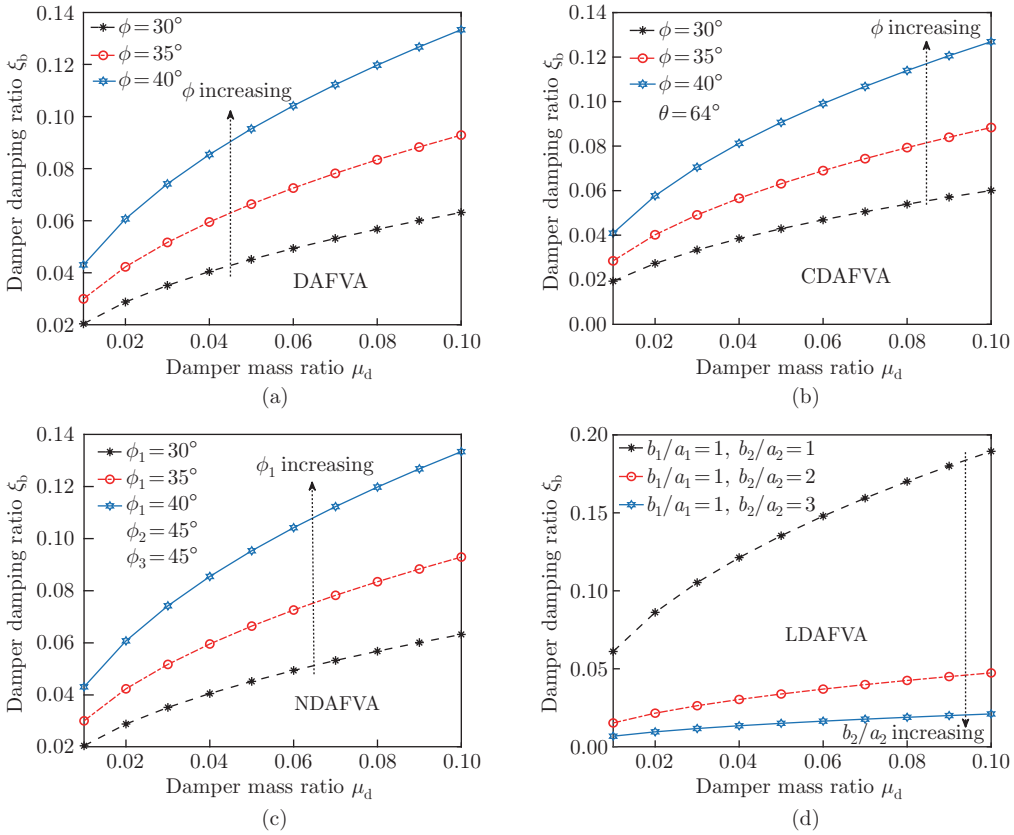

Fig. 8 Variations in the optimal damping ratio of the (a) DAFVA, (b) CDAFVA, (c) NDAFVA, and (d) LDAFVA as a function of the mass ratio of the damper (color online)

are first deployed. Tables 1 and 2 contain the governing system parameters for the H_2 optimized vibration absorbers and the SDOF systems. These optimal design parameters and the FRFs created in the preceding sections are used to derive the optimal displacements of the controlled SDOF systems. The optimum conventional vibration absorbers are used to estimate the superior vibration reduction performance of the novel dampers. The conventional TMD's controlling system parameters are borrowed from two reputable articles. In Table 2, the paper is cited. To conduct a fair comparison between the vibration reduction performances of the novel vibration absorbers and the conventional vibration absorbers, the mass ratios of both are kept exactly the same. Currently, after employing all system parameters, the differences between the frequency ratio and the optimal displacements of the SDOF systems controlled by the H_2 optimized DAFVAs, CDAFVAs, NDAFVAs, and LDAFVAs are obtained and graphically displayed in Figs. 9(a), 9(b), 9(c), and 9(d), respectively.

Table 1 The structural system parameter for the SDOF system

Primary structure	Governing system parameter	Value ξ_s
SDOF	Damping ratio	0.01

Using the FRF, the maximum displacement response of the uncontrolled SDOF system is likewise calculated analytically; the value achieved is 50. The SDOF systems controlled by H_2 optimized DAFVAs, CDAFVAs, NDAFVAs, and LDAFVAs yield the following maximum displacement response: 6.476 1. Meanwhile, 8.017 7 and 7.505 5 are the maximum displacement

Table 2 The novel and conventional TMD's H_2 optimized design parameters

System	Reference	H_2 optimization	
		κ_b	ξ_b
DAFVA	Present	0.940 401	0.077 313 2
CDAFVA	Present	0.940 401	0.073 566 0
NDAFVA	Present	0.940 401	0.077 313 2
LDAFVA	Present	0.940 401	0.109 806 0
Conventional TMD1	Refs. [25] and [26]	$\frac{1}{\sqrt{1+\tilde{\mu}_d}}$	$\frac{\sqrt{\tilde{\mu}_d}}{2}$
Conventional TMD2	Refs. [25] and [27]	$\frac{1}{1+\tilde{\mu}_d}\sqrt{\frac{2+\tilde{\mu}_d}{2}}$	$\sqrt{\frac{\tilde{\mu}_d(4+3\tilde{\mu}_d)}{8(1+\tilde{\mu}_d)(2+\tilde{\mu}_d)}}$

Conventional TMD1: damper mass ratio ($\tilde{\mu}_d$) = 0.05; conventional TMD2: damper mass ratio ($\tilde{\mu}_d$) = 0.05; DAFVAs: damper mass ratio (μ_d) = 0.05, ϕ = 40°; CDAFVAs: μ_d = 0.05, ϕ = 40°, θ = 64°; NDAFVAs: μ_d = 0.05, ϕ_1 = 40°, ϕ_2 = 45°, ϕ_3 = 45°; LDAFVAs: μ_d = 0.05, $b_1/a_1 = 1$, $b_2/a_2 = 1$

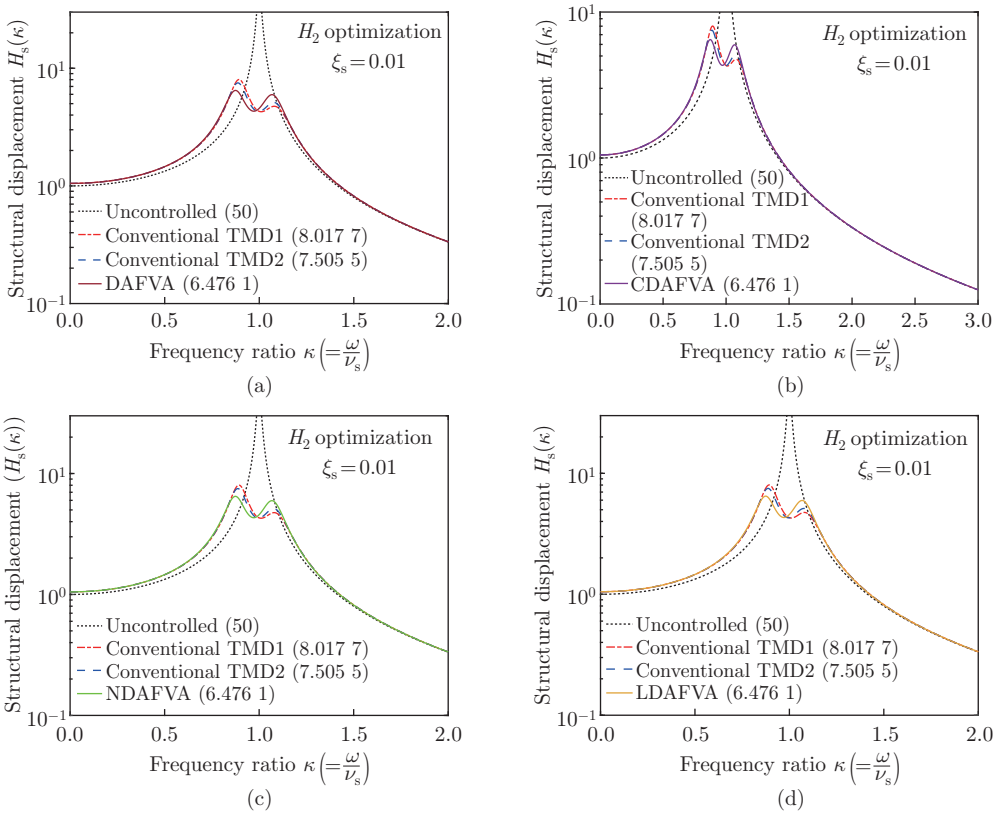

Fig. 9 Variations in the optimal displacements of the SDOF systems controlled by the H_2 optimized (a) DAFVA, (b) CDAFVA, (c) NDAFVA, and (d) LDAFVA as a function of the frequency ratio of the excitation (color online)

responses of the systems with an SDOF that is controlled using a conventional TMD. The vibration reduction capacities of the novel vibration absorbers are derived with respect to the conventional TMD, and the mathematical expression for the required derivation is as follows:

$$H_{dr} = \left(\frac{(H_s(\kappa))_{\text{conventional}} - (H_s(\kappa))_{\text{novel}}}{(H_s(\kappa))_{\text{conventional}}}\right) \times 100\%, \tag{43}$$

where $(H_s(\kappa))_{\text{conventional}}$ and $(H_s(\kappa))_{\text{novel}}$ define the maximum displacements of the SDOF

system controlled by the conventional and the novel vibration absorbers, respectively. The maximum displacement responses of the SDOF systems isolated by H_2 optimized DAFVAs, CDAFVAs, NDAFVAs, and LDAFVAs are applied to Eq. (43). Accordingly, the vibration reduction capacities of the DAFVAs, CDAFVAs, NDAFVAs, and LDAFVAs are 19.23% and 13.71 %, superior to the conventional vibration absorbers one and two. Similarly, this vibration reduction capacity is derived for the H_∞ novel vibration absorbers. To perform the analytical study, the H_∞ optimized design parameters for the novel vibration absorbers are derived using Eq. (38), Eq. (39), Eq. (40), Eq. (41), and Eq. (42). The design parameters for the conventional vibration absorbers are obtained from published journals. The details of all system parameters for optimum novel and conventional vibration absorbers are listed in Table 3. To conduct a fair comparison between the vibration reduction performances of the novel vibration absorbers and the conventional vibration absorbers, the mass ratios of both are kept exactly the same. The differences in the optimal displacements of the SDOF systems controlled by the H_∞ optimized DAFVAs, CDAFVAs, NDAFVAs, and LDAFVAs in relation to the frequency ratio are now obtained and graphically presented in Figs. 10(a)–10(d) after all system parameters have been applied. The FRF is also used to analytically determine the maximum displacement response of the uncontrolled SDOF system, and the result is 50. The H_∞ optimized DAFVAs, CDAFVAs, NDAFVAs, and LDAFVAs controlled SDOF systems yield the following maximum displacement responses: 6.171 2. The SDOF system controlled by the conventional vibration absorbers yields the maximum displacement responses of 6.632 5 and 6.621 5. Using Eq. (43), the vibration reduction capacities of the suggested vibration absorbers are calculated in relation to the conventional vibration absorbers. As a result, the H_∞ optimized DAFVAs, CDAFVAs, NDAFVAs, and LDAFVAs are 6.95% and 6.8% more capable of reducing vibration than the conventional vibration absorbers.

Table 3 The values of each H_∞ optimized design parameter for conventional and novel vibration absorbers

System	Reference	H_∞ optimization	
		κ_b	ξ_b
DAFVA	Present	0.940 401	0.095 286 4
CDAFVA	Present	0.940 401	0.090 668 1
NDAFVA	Present	0.940 401	0.095 286 4
LDAFVA	Present	0.940 401	0.135 333 0
Conventional TMD1	Refs. [28] and [29]	$\frac{1}{1+\tilde{\mu}_\mathrm{d}}$	$\sqrt{\frac{3\tilde{\mu}_\mathrm{d}}{8(1+\tilde{\mu}_\mathrm{d})}}$
Conventional TMD2	Ref. [30]	$\frac{1}{1+\tilde{\mu}_\mathrm{d}}$	$\sqrt{\frac{\tilde{\mu}_\mathrm{d}}{2(1+\tilde{\mu}_\mathrm{d})}}$

Conventional TMD1: damper mass ratio ($\tilde{\mu}_\mathrm{d}$) = 0.05; conventional TMD2: damper mass ratio ($\tilde{\mu}_\mathrm{d}$) = 0.05; DAFVAs: damper mass ratio (μ_d) = 0.05, $\phi = 40^\mathrm{o}$; CDAFVAs: $\mu_\mathrm{d} = 0.05$, $\phi = 40^\mathrm{o}$, $\theta = 64^\mathrm{o}$; NDAFVAs: $\mu_\mathrm{d} = 0.05$, $\phi_1 = 40^\mathrm{o}$, $\phi_2 = 45^\mathrm{o}$, $\phi_3 = 45^\mathrm{o}$; LDAFVAs: $\mu_\mathrm{d} = 0.05$, $b_1/a_1 = 1$, $b_2/a_2 = 1$

The additional tests are intended to validate the proposed methodology in a wider variety of seismic excitation conditions. In order to do this, the Clough-Penzien power spectrum, a modified variant of the well-known Kanai-Tajimi spectrum, might serve as the study's ground acceleration. The process is distinct since it makes use of a one-sided power spectral density,

$$\begin{aligned} U_{\ddot{u}_\mathrm{g}} &= S_0 \frac{\epsilon_\mathrm{f}^4 + 4\zeta_\mathrm{f}^2\epsilon_\mathrm{f}^2\omega^2}{(\epsilon_\mathrm{f}^2 - \omega^2)^2 + 4\zeta_\mathrm{f}^2\epsilon_\mathrm{f}^2\omega^2} \frac{\omega^4}{(\epsilon_\mathrm{g}^2 - \omega^2)^2 + 4\zeta_\mathrm{g}^2\epsilon_\mathrm{g}^2\omega^2} \\ &= S_0 \frac{\epsilon_\mathrm{f}^4 - 4\zeta_\mathrm{f}^2\epsilon_\mathrm{f}^2 q^2}{(\epsilon_\mathrm{f}^2 + q^2)^2 - 4\zeta_\mathrm{f}^2\epsilon_\mathrm{f}^2 q^2} \frac{q^4}{(\epsilon_\mathrm{g}^2 + q^2)^2 - 4\zeta_\mathrm{g}^2\epsilon_\mathrm{g}^2 q^2}, \end{aligned} \tag{44}$$

where the constant power spectral density for random white noise excitation is defined by S_0, and $q = \mathrm{i}\omega$. The well-known Kanai-Tajimi model's filter parameters are ϵ_f for the soil

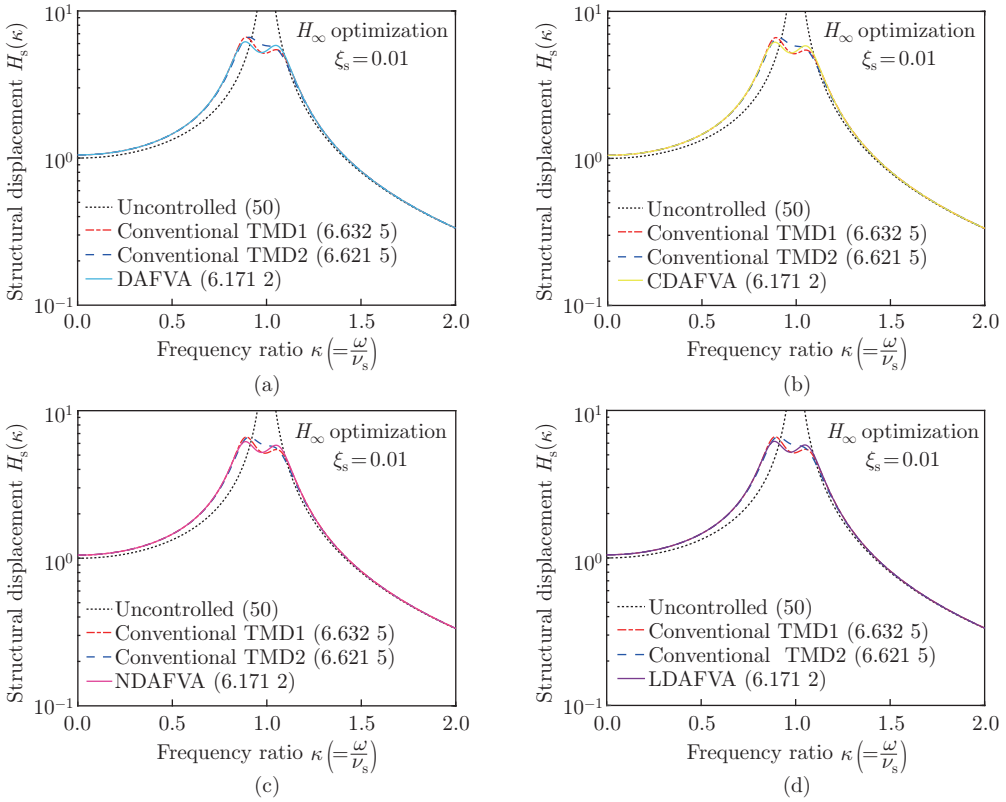

Fig. 10 Variations in the optimal displacements of the SDOF systems controlled by the H_∞ optimized (a) DAFVA, (b) CDAFVA, (c) NDAFVA, and (d) LDAFVA as a function of the frequency ratio of the excitation (color online)

layer's natural frequency and ζ_f for the soil layer's damping capacity. A second filter with the parameters ϵ_g and ζ_g produces a limited power output for the ground displacement. The second filter only takes into account very low range frequencies since the second quotient $\epsilon_g \ll \epsilon_f$ hits unity very quickly. Reference [31] provides the filter parameter values for the research locations with firm, medium, and soft soils. In this study, firm soil is considered.

The variations of optimal displacements of the SDOF systems controlled by the H_2 optimized DAFVAs, CDAFVAs, NDAFVAs, and LDAFVAs as a function of the frequency ratio under the random-white excitation have been shown in Fig. 11(a). The maximum displacement of the uncontrolled structure is obtained as $1.411\,3 \times 10^6$ dB/Hz. The maximum displacements of the structure controlled by conventional TMD1, conventional TMD2, DAFVAs, CDAFVAs, NDAFVAs, and LDAFVAs are obtained as $1.234\,8 \times 10^6$ dB/Hz, $1.068\,6 \times 10^6$ dB/Hz, $8.153\,8 \times 10^5$ dB/Hz, $9.613\,7 \times 10^5$ dB/Hz, $8.242\,5 \times 10^5$ dB/Hz, and $7.924\,3 \times 10^5$ dB/Hz. Hence, the DAFVAs, CDAFVAs, NDAFVAs, and LDAFVAs are 33.96%, 22.14%, 33.24%, and 35.82% superior to the conventional TMDs. The variations of optimal displacements of the SDOF systems controlled by the H_∞ optimized DAFVAs, CDAFVAs, NDAFVAs, and LDAFVAs as a function of the frequency ratio under the random-white excitation have been shown in Fig. 11(b). The maximum displacement of the uncontrolled structure is obtained as $1.482\,7 \times 10^6$ dB/Hz. The maximum displacements of the structure controlled by conventional TMD1, conventional TMD2, DAFVAs, CDAFVAs, NDAFVAs, and LDAFVAs are obtained as 9.063×10^5 dB/Hz, $8.912\,5 \times 10^5$ dB/Hz, $7.168\,3 \times 10^5$ dB/Hz, 7.616×10^5 dB/Hz, 7.765×10^5 dB/Hz, and 8.505×10^5 dB/Hz. Hence, the DAFVAs, CDAFVAs, NDAFVAs, and LDAFVAs are 20.9%, 15.96%, 14.31%, and 6.15% superior to the conventional TMDs. To highlight the advantages of the

damping amplification mechanism of the novel absorbers, a comparison is conducted with a conventional vibration absorber containing a spring and dry friction damping[24]. The optimal design parameters of FTMD are taken from a published paper and listed in Table 4. The total mass of each damper is considered the same. The variations in the optimal displacements of the SDOF systems controlled by the H_2 and H_∞ optimized DAFVA, CDAFVA, NDAFVA, and LDAFVA as a function of the frequency ratio under the harmonic excitation are shown in Figs. 12(a), 12(b), 12(c), and 12(d), respectively. α is set to 0.2. The maximum displacement of an uncontrolled SDOF system is determined as 50. The maximum displacement of the SDOF system controlled by the FTMD is determined as 21.191 6. The maximum displacements of the SDOF system controlled by H_2 and H_∞ optimized DAFVAs are determined as 6.455 4 and 6.166 6. Accordingly, the H_2 and H_∞ optimized DAFVAs are 69.537 9% and 70.900 6% superior to the FTMD. The maximum displacements of the SDOF system controlled by H_2 and H_∞ optimized CDAFVAs are determined as 6.455 4 and 6.166 6. Accordingly, the H_2 and H_∞ optimized CDAFVAs are 69.537 9% and 70.900 6% superior to the FTMD. The maximum displacements of the SDOF system controlled by H_2 and H_∞ optimized NDAFVAs are determined as 6.455 4 and 6.166 6. Accordingly, the H_2 and H_∞ optimized NDAFVAs are 69.537 9% and 70.900 6% superior to the FTMD. The maximum displacements of the SDOF system controlled by H_2 and H_∞ optimized LDAFVAs are determined as 6.455 4 and 6.166 6. Accordingly, the H_2 and H_∞ optimized LDAFVAs are 69.537 8% and 70.900 7% superior to the FTMD.

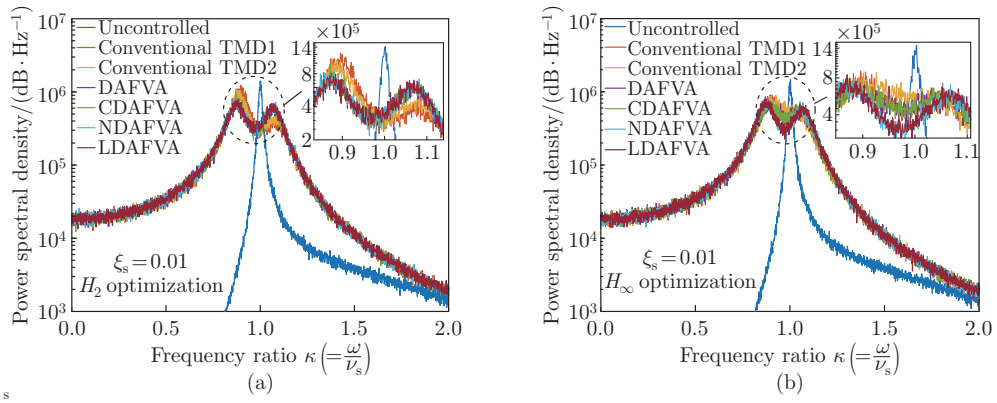

Fig. 11 Variations in the optimal displacements of the SDOF systems controlled by the (a) H_2 and (b) H_∞ optimized DAFVAs, CDAFVAs, NDAFVAs, and LDAFVAs as a function of the frequency ratio under the random-white excitation (color online)

Table 4 The optimal design parameters of FTMD

System	Reference	Optimal parameter	
		κ_b	ξ_b
FTMD	Ref. [24]	1	0.029 1

The random excitation is applied at the base of the controlled structures to simulate real-world dynamic loads, such as seismic ground motion and environmental vibrations. This approach helps assess the effectiveness of control strategies in mitigating structural responses under uncertain and unpredictable loading conditions. The variations in the optimal displacements of the SDOF systems controlled by the H_2 and H_∞ optimized DAFVAs, CDAFVAs, NDAFVAs, and LDAFVAs as a function of the frequency ratio under the random excitation are shown in Figs. 13(a), 13(b), 13(c), and 13(d). The maximum displacement of an uncontrolled SDOF system is determined as $3.261\,7 \times 10^7$ dB/Hz. The maximum displacement of the

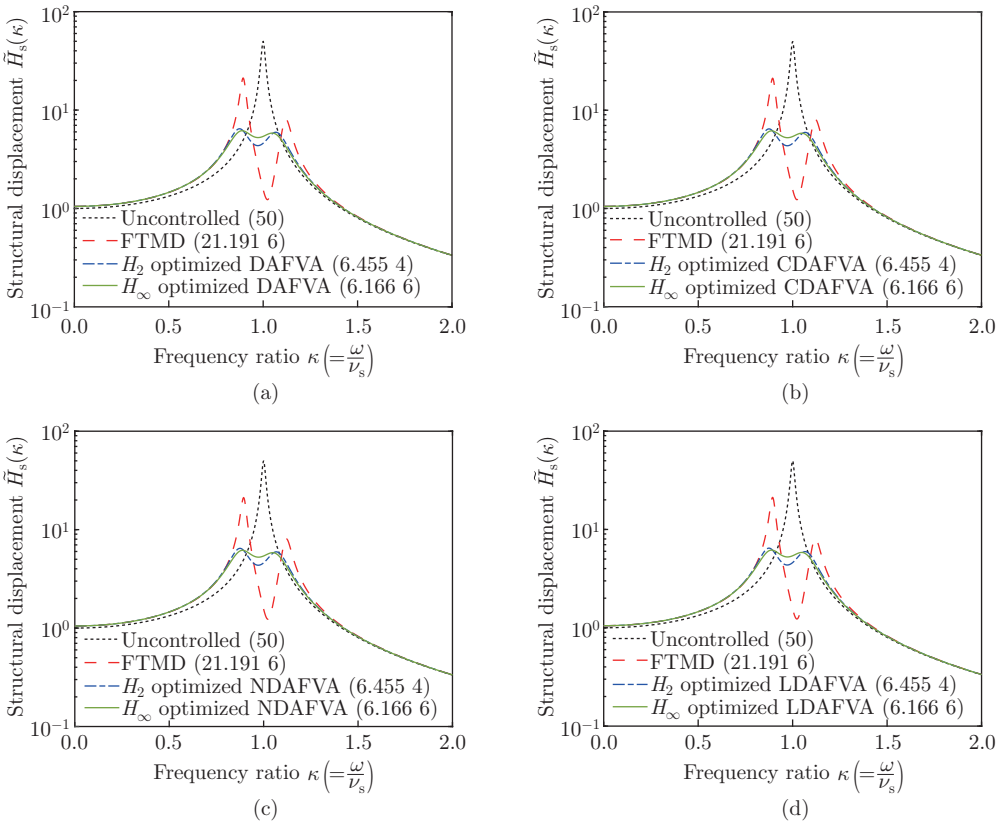

Fig. 12 Variations in the optimal displacements of the SDOF systems controlled by the H_2 and H_∞ optimized (a) DAFVA, (b) CDAFVA, (c) NDAFVA, and (d) LDAFVA as a function of the frequency ratio under the harmonic excitation (color online)

SDOF system controlled by the FTMD is determined as $6.249\,7 \times 10^6$ dB/Hz. The maximum displacements of the SDOF system controlled by H_2 and H_∞ optimized DAFVAs are determined as $5.711\,5 \times 10^5$ dB/Hz and $5.637\,7 \times 10^5$ dB/Hz. Accordingly, the H_2 and H_∞ optimized DAFVAs are 90.861 1% and 90.979 2% superior to the FTMD. The maximum displacement of the SDOF system controlled by the FTMD is determined as $6.081\,7 \times 10^6$ dB/Hz. The maximum displacements of the SDOF system controlled by H_2 and H_∞ optimized CDAFVAs are determined as $6.564\,8 \times 10^5$ dB/Hz and 5.402×10^5 dB/Hz. Accordingly, the H_2 and H_∞ optimized CDAFVAs are 89.205 8% and 91.117 7% superior to the FTMD. The maximum displacement of the SDOF system controlled by the FTMD is determined as $6.602\,8 \times 10^6$ dB/Hz. The maximum displacements of the SDOF system controlled by H_2 and H_∞ optimized NDAFVAs are determined as $6.034\,9 \times 10^5$ dB/Hz and $5.503\,5 \times 10^5$ dB/Hz. Accordingly, the H_2 and H_∞ optimized NDAFVAs are 90.860 1% and 91.664 9% superior to the FTMD. The maximum displacement of the SDOF system controlled by the FTMD is determined as $6.128\,6 \times 10^6$ dB/Hz. The maximum displacements of the SDOF system controlled by H_2 and H_∞ optimized LDAFVAs are determined as $5.816\,8 \times 10^5$ dB/Hz and $5.144\,8 \times 10^5$ dB/Hz. Accordingly, the H_2 and H_∞ optimized LDAFVAs are 90.508 8% and 91.605 3% superior to the FTMD. Figures 14(a), 14(b), 14(c), and 14(d) illustrate the variations in optimal displacements of SDOF systems controlled by different absorber configurations: DAFVA, CDAFVA, NDAFVA, and LDAFVA.

The structural displacement is plotted against the frequency ratio, revealing how different parameter choices influence vibration mitigation. In DAFVA, CDAFVA, and NDAFVA, increasing ϕ and ϕ_1 generally reduces the resonance peak, with $\phi = 40°$ and $\phi_1 = 40°$ showing

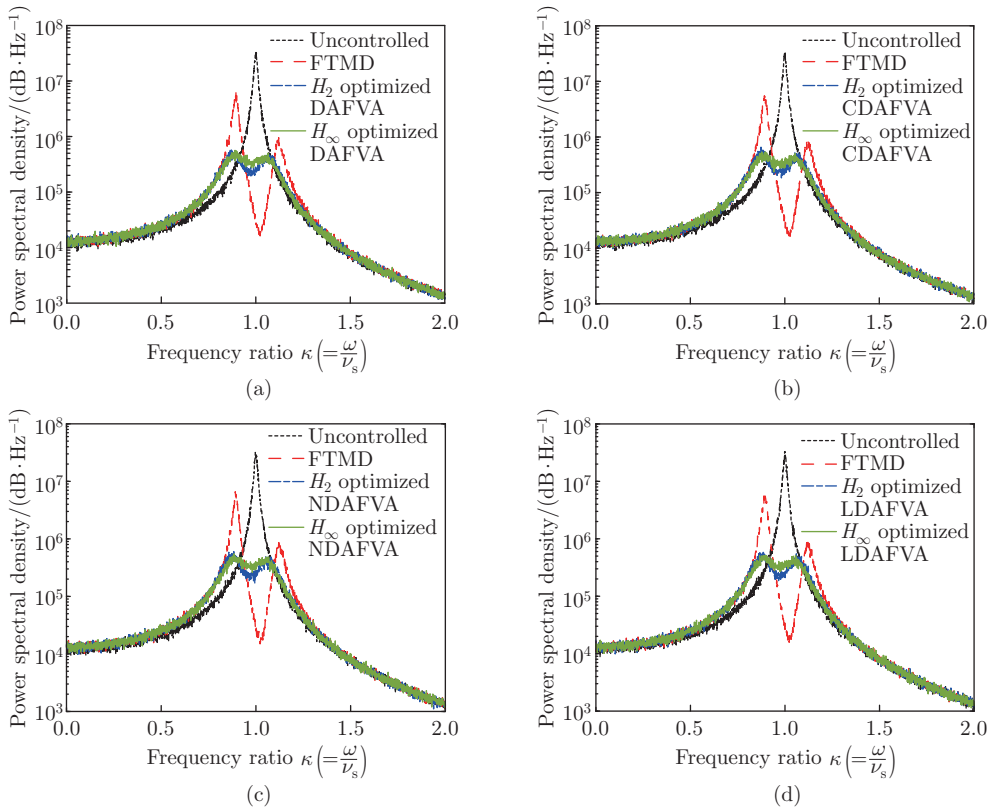

Fig. 13 Variations in the optimal displacements of the SDOF systems controlled by the (a) H_2 and (b) H_∞ optimized DAFVA, CDAFVA, NDAFVA, and LDAFVA as a function of the frequency ratio of the random excitation (color online)

the most effective suppression. LDAFVA, on the other hand, is analyzed for different values of L_2, where lower values significantly dampen the peak displacement, demonstrating its superior ability to mitigate vibrations. Comparatively, LDAFVA exhibits the most effective performance in resonance suppression, followed by NDAFVA and CDAFVA, while DAFVA shows the highest peak, indicating lower efficiency. Overall, the results emphasize the importance of parameter tuning, where increasing ϕ, ϕ_1, and decreasing L_2 enhance the absorber's effectiveness in reducing structural vibrations.

4 Summary and conclusions

The paper introduces and analyzes a novel class of DAFVAs to enhance vibration mitigation in structural systems. Using H_2 and H_∞ optimization approaches, closed-form analytical solutions for optimal design parameters are derived, and their effectiveness is verified through numerical simulations. The results demonstrate that the proposed absorbers significantly outperform conventional FTMDs and traditional TMDs, achieving superior vibration reduction while maintaining robustness across various dynamic conditions. The paper introduces an innovative vibration control mechanism by integrating damping amplification into friction-based vibration absorbers, offering a significant advancement over conventional TMDs. The study introduces a key innovation by incorporating damping amplifiers into conventional vibration absorbers, which fundamentally enhances their energy dissipation capacity. The distinct novelty of our approach is as follows:

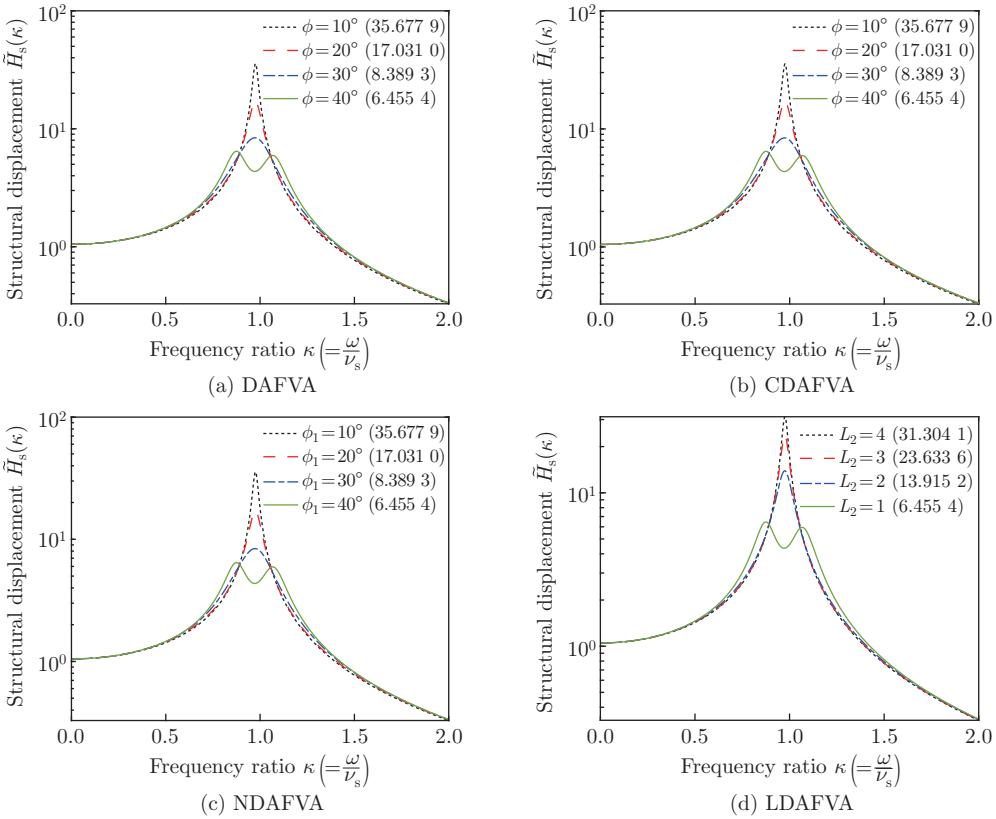

Fig. 14 Variations in the optimal displacements of the SDOF systems controlled by the optimum (a) DAFVA, (b) CDAFVA, (c) NDAFVA, and (d) LDAFVA as a function of the frequency ratio for different values of ϕ, ϕ_1, and $L_2 = \frac{b_2}{a_2}$ (color online)

(i) Nonlinear damping amplification: unlike traditional Voigt-type dynamic vibration absorbers, which rely on increasing both static damping and mass to enhance vibration attenuation, our proposed absorbers leverage damping amplification mechanisms to achieve superior performances without such increases. Conventional Voigt-type dynamic vibration absorbers exhibit limited vibration reduction capacity when static damping remains low, often necessitating multiple absorbers to achieve effective mitigation. In contrast, our novel absorbers efficiently enhance vibration attenuation through amplified damping effects, enabling a single unit to provide robust vibration control while maintaining a compact and efficient design.

(ii) Multiple configurations for enhanced performance: the four proposed absorbers, i.e., DAFVAs, CDAFVAs, NDAFVAs, and LDAFVAs utilize distinct amplification strategies, each tailored to optimize vibration reduction performance. These configurations introduce varying degrees of frequency tuning and damping enhancement, allowing for greater adaptability to different structural requirements. By leveraging unique damping amplification mechanisms, each design provides a tailored approach to improving vibration mitigation efficiency beyond conventional absorbers.

(iii) Closed-form optimized design: unlike traditional dynamic vibration absorbers, which rely on empirical tuning, our approach derives closed-form analytical expressions for optimal damping and stiffness parameters using H_2 and H_∞ optimization techniques. These formulations enable precise tuning, ensuring optimal vibration suppression across both harmonic and random excitations. By providing mathematically rigorous design parameters, our method enhances performance predictability and efficiency, eliminating the trial-and-error approach

commonly associated with conventional absorbers.

(iv) Superior vibration reduction performance: the effectiveness of our proposed designs is rigorously validated through comprehensive analytical and numerical studies, demonstrating a substantial improvement over conventional TMDs. Specifically, our optimized absorbers achieve 91.605 3% greater vibration attenuation compared with the best-performing conventional FTMD, highlighting their enhanced efficiency and robustness in mitigating structural vibrations.

(v) Nonlinear frictional damping contribution: our proposed absorbers utilize a frictional element to generate nonlinear frictional forces, enhancing vibration attenuation through controlled energy dissipation. This nonlinear damping mechanism significantly improves performance under broadband excitations, enabling superior vibration reduction compared with conventional absorbers that rely solely on linear damping. By effectively leveraging frictional damping, our design achieves optimal vibration control while maintaining structural efficiency.

In summary, while the fundamental layout of a vibration absorber remains, this study contributes significantly by incorporating damping amplification mechanisms, providing closed-form optimal design solutions, and demonstrating superior vibration reduction capabilities. The proposed DAFVAs offer a transformative approach to structural vibration control, potentially reducing material costs, improving structural resilience, and extending the lifespan of engineering structures. Their adaptability to different vibration conditions makes them a viable alternative to conventional TMDs, bridging the gap between theoretical advancements and real-world applications in infrastructure. The future work will involve prototype fabrication, experimental testing, and comparison with the theoretical and numerical results to further confirm the effectiveness of the proposed method.

Conflict of interest The authors declare no conflict of interest.

Acknowledgements The authors would like to acknowledge the postdoctoral research grant received from the University of Glasgow for the partial financial support for this research work.

References

[1] LERNER, A. A. and CUNEFARE, K. Performance of mre-based vibration absorbers. *Journal of Intelligent Material Systems and Structures*, **19**(5), 551–563 (2008)

[2] LIU, K. and LIU, J. The damped dynamic vibration absorbers: revisited and new result. *Journal of Sound and Vibration*, **284**(3-5), 1181–1189 (2005)

[3] YANG, C., LI, D., and CHENG, L. Dynamic vibration absorbers for vibration control within a frequency band. *Journal of Sound and Vibration*, **330**(8), 1582–1598 (2011)

[4] WAGNER, N. and HELFRICH, R. Dynamic vibration absorbers and its applications. *Journal of Sound and Vibration*, **354**, 6 (2017)

[5] MORADI, H., BAKHTIARI-NEJAD, F., and MOVAHHEDY, M. R. Tuneable vibration absorber design to suppress vibrations: an application in boring manufacturing process. *Journal of Sound and Vibration*, **318**(1-2), 93–108 (2008)

[6] ALOTTA, G. and FAILLA, G. Improved inerter-based vibration absorbers. *International Journal of Mechanical Sciences*, **192**, 106087 (2021)

[7] CERA, M., CIRELLI, M., PENNESTRÌ, E., and VALENTINI, P. P. Design analysis of torsichrone centrifugal pendulum vibration absorbers. *Nonlinear Dynamics*, **104**, 1023–1041 (2021)

[8] MAHÉ, V., RENAULT, A., GROLET, A., MAHÉ, H., and THOMAS, O. On the dynamic stability and efficiency of centrifugal pendulum vibration absorbers with rotating pendulums. *Journal of Sound and Vibration*, **536**, 117157 (2022)

[9] LI, H., TOUZÉ, C., PELAT, A., and GAUTIER, F. Combining nonlinear vibration absorbers and the acoustic black hole for passive broadband flexural vibration mitigation. *International Journal of Non-Linear Mechanics*, **129**, 103558 (2021)

[10] MAYET, J., ACAR, M. A., and SHAW, S. W. Effective and robust rocking centrifugal pendulum vibration absorbers. *Journal of Sound and Vibration*, **527**, 116821 (2022)

[11] GOMEZ, E. R., ARTEAGA, I. L., and KARI, L. Normal-force dependant friction in centrifugal pendulum vibration absorbers: simulation and experimental investigations. *Journal of Sound and Vibration*, **492**, 115815 (2021)

[12] CHANG, Y., ZHOU, J., WANG, K., and XU, D. A quasi-zero-stiffness dynamic vibration absorber. *Journal of Sound and Vibration*, **494**, 115859 (2021)

[13] YOU, T., ZHOU, J., THOMPSON, D. J., GONG, D., CHEN, J., and SUN, Y. Vibration reduction of a high-speed train floor using multiple dynamic vibration absorbers. *Vehicle System Dynamics*, **60**(9), 2919–2940 (2022)

[14] CHOWDHURY, S. and BANERJEE, A. The impacting vibration absorbers. *Applied Mathematical Modelling*, **127**, 454–505 (2024)

[15] SU, N., CHEN, Z., XIA, Y., and BIAN, J. Hybrid analytical h-norm optimization approach for dynamic vibration absorbers. *International Journal of Mechanical Sciences*, **264**, 108796 (2024)

[16] SU, N., BIAN, J., PENG, S., CHEN, Z., and XIA, Y. Analytical optimal design of inerter-based vibration absorbers with negative stiffness balancing static amplification and dynamic reduction effects. *Mechanical Systems and Signal Processing*, **192**, 110235 (2023)

[17] ZHANG, Y., CHENG, J., XU, W., WANG, C., LIU, J., LI, Y., and YANG, S. Particle damping vibration absorber and its application in underwater ship. *Journal of Vibration Engineering & Technologies*, **11**(5), 2231–2248 (2023)

[18] GUO, M., TANG, L., WANG, H., LIU, H., and GAO, S. A comparative study on transient vibration suppression of magnetic nonlinear vibration absorbers with different arrangements. *Nonlinear Dynamics*, **111**(18), 16729–16776 (2023)

[19] SU, N., BIAN, J., CHEN, Z., and XIA, Y. A novel 550 lever-type inerter-based vibration absorber. *International Journal of Mechanical Sciences*, **254**, 108440 (2023)

[20] ZHAO, C., ZHANG, K., ZHAO, P., and DENG, Z. Finite-amplitude nonlinear waves in inertial amplification metamaterials: theoretical and numerical analyses. *Journal of Sound and Vibration*, **560**, 117802 (2023)

[21] ZHAO, C., ZHANG, K., ZHAO, P., HONG, F., and DENG, Z. Bandgap merging and backward wave propagation in inertial amplification metamaterials. *International Journal of Mechanical Sciences*, **250**, 108319 (2023)

[22] MA, H., CHENG, Z., SHI, Z., and MARZANI, A. Structural vibration mitigation via an inertial amplification mechanism based absorber. *Engineering Structures*, **295**, 116764 (2023)

[23] SETTIMI, V., LEPIDI, M., and BACIGALUPO, A. Analytical spectral design of mechanical metamaterials with inertia amplification. *Engineering Structures*, **274**, 115054 (2023)

[24] GEWEI, Z. and BASU, B. A study on friction-tuned mass damper: harmonic solution and statistical linearization. *Journal of Vibration and Control*, **17**(5), 721–731 (2011)

[25] WARBURTON, G. B. Optimum absorber parameters for various combinations of response and excitation parameters. *Earthquake Engineering & Structural Dynamics*, **10**(3), 381–401 (1982)

[26] ZILLETTI, M., ELLIOTT, S. J., and RUSTIGHI, E. Optimisation of dynamic vibration absorbers to minimise kinetic energy and maximise internal power dissipation. *Journal of Sound and Vibration*, **331**(18), 4093–4100 (2012)

[27] IWATA, Y. On the construction of the dynamic vibration absorbers. *Japanese Society of Mechanical Engineering*, **820**(8), 150–152 (1982)

[28] ORMONDROYD, J. and DEN HARTOG, J. P. The theory of the dynamic vibration absorber. *Journal of Fluids Engineering*, **49**(2), 021007 (1928)

[29] NISHIHARA, O. and ASAMI, T. Closed-form solutions to the exact optimizations of dynamic vibration absorbers (minimizations of the maximum amplitude magnification factors). *Journal of Vibration and Acoustics*, **124**(4), 576–582 (2002)

[30] KRENK, S. Frequency analysis of the tuned mass damper. *Journal of Applied Mechanics*, **72**, 936–942 (2005)

[31] KIUREGHIAN, A. D. and NEUENHOFER, A. Response spectrum method for multi-support seismic excitations. *Earthquake Engineering & Structural Dynamics*, **21**(8), 713–740 (1992)